Geosciences Journal
Vol. 20, No. 4, p. 427 − 447, August 2016
DOI 10.1007/s12303-015-0062-x

U-Pb zircon systematics of the Mansehra Granitic Complex: implications on the early Paleozoic orogenesis in NW Himalaya of Pakistan

Mustansar Naeem
Jean-Pierre Burg

Institute of Geology, University of the Punjab, Quaid-e-Azam Campus, Lahore 54590, Pakistan
Department of Earth Sciences, Eidgenössische Technische Hochschule Zürich (ETH-Zurich), Zürich 8092, Switzerland

Nasir Ahmad
Muhammed Nawaz Chaudhry
Perveiz Khalid*

Institute of Geology, University of the Punjab, Quaid-e-Azam Campus, Lahore 54590, Pakistan

ABSTRACT: Mansehra Granitic Complex (MGC) lies in the NW Himalaya of Pakistan. The MGC magmatic rocks are peraluminous, calc-alkaline S-type granitoids. Prior to this study the Mansehra Granite had produced ages of 83 Ma by K/Ar, 215 Ma using Ar/Ar on biotite, and 516 ± 16 Ma, using the whole rock Rb/Sr method. The Susalgali Granite Gneiss, a sheared facies of the Mansehra Granite previously regarded as older than the Mansehra Granite, was dated at 79 Ma using K/Ar on biotite. Hakale Granite, which is intrusive into the Mansehra Granite, had yielded K/Ar muscovite age of 165 Ma. The age of the leucogranites was not reported before this contribution. We have presented the revised geochronology of the MGC magmatic bodies, employing SHRIMP and LA-ICP-MS U-Pb zircon chronometry, to constraint precise crystallization ages and tectonic setting of the NW Himalaya, Pakistan. Dates of emplacement of the Mansehra Granite, leucogranites and Hakale Granite are ca. 478, 475 and 466 Ma, respectively. These new ages are comparable to U-Pb zircon and Rb/Sr dates of other granites and granite gneisses in the Lesser Himalaya to the east, in India, Nepal, south Tibet and SW China. The age components of ca. 1900–1300, 985–920, 880–800 and 690–500 Ma are interpreted as inherited grains. Geochronological and field evidence suggest that the MGC of the NW Himalaya are the product of an Andean-type Cambro-Ordovician accretional orogenesis with continental-continental settings along the northen margin of east Gondwana. On the basis of new age data of the MGC plutonic rocks it is inferred that Cambro-Ordovician accretional event commenced from SW China and extends at least up to NW Pakistan along the northern margin of east Gondwana. However, granitic rocks of Pan African affiliation prevail in central Iran and Turkey along northern and western margins of Gondwana.

Key words: Mansehra Granitic Complex, S-type granitoids, U-Pb zircon chronometry, SHRIMP, LA-ICP-MS techniques, Gondwana, Pan African, Cambro-Ordovician

1. INTRODUCTION

The Himalayan mountain range is about 2500 km long in the East-West direction (Fig. 1). Western part of this range lies in Pakistan which is characterized by intense deformation, metamorphism, thrusting and plutonism (Baig et al., 1989; Virjan et al., 2003). Magmatic bodies exposed in the NW Himalaya of Pakistan are named Mansehra Granitic Complex (MGC) (Fig. 2). The rocks of this Complex are comprised of Mansehra Granite (MG), Hakale Granite (HG), pegmatites, aplites and leucogranitic (LG) bodies (Shams, 1961; 1967; 1971; Ashraf, 1974; Ashraf and Chaudhry, 1976a, 1976b; Naeem, 2013). Granitic bodies emplaced along the Himalayan orogenic belt were previously assigned Paleozoic to late Cenozoic ages on the basis of field relationships, nature of xenoliths, structural trends, geochronological and geochemical investigations, petrological properties, and degree of metamorphism (McMahon, 1884; Greisbach, 1893; Hayden, 1913; Auden, 1932; Wadia, 1928, 1957). However, Shams (1967) dated the "Susalgali Granite Gneiss" at 79 Ma using K/Ar isotope systematic on biotite, which is interpreted as sheared Mansehra Granite, and the main body of the Mansehra Granite at 83 Ma. He also dated the Hakale Granite muscovite by K/Ar technique at 165 Ma. However, these ages are inconsistent with the field relations of these rocks. The Hakale Granite was assigned an older age but intrudes the Mansehra Granite suggesting that it is unlikely to be 516 ± 16 Ma as reported by Le Fort et al. (1980). Maluski and Matte (1984) produced an age of 215 Ma of MG by using Ar/Ar method on biotite. However, the age of the leucogranites was not determined prior to this study. Radiometric dates of the MGC magmatic bodies are poorly understood and their relationship with time-equivalent plutonic rocks of the Himalaya in India, Nepal and Tibet Plateau is not clearly known. We are presenting the revised U-Pb zircon ages of the MGC plutonic rocks. In situ zircon U/Pb is one of the most robust methods for yielding magmatic ages of silicic igneous rocks.We have used Sensitive High Resolution Ion Microprobe (SHRIMP) and Laser Ablation Inductively Coupled Plasma Mass Spectrometer (LA-ICP-MS) to measure the U-Pb ratio for high precision zircon geochronology of the MGC. The new U-Pb zircon ages of the MGC magmatic bodies will contribute to unravel their petrogenesis and tectonic setting along the northern margin of Gondwana. Results of the study integrated with previous work will furnish new evidence of an early

*Corresponding author: perveiz.geo@pu.edu.pk

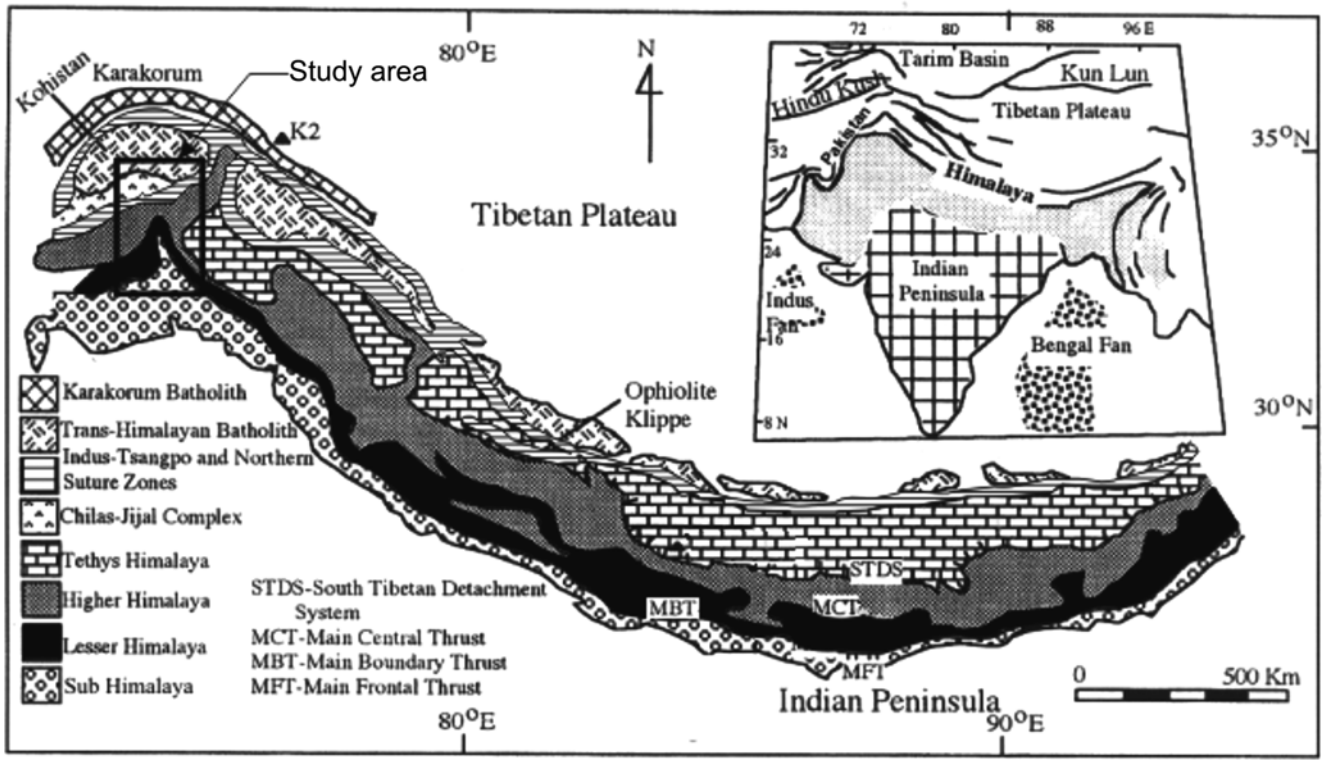

Fig. 1. Geological map of the Himalaya indicating major tectonic divisions (modified from Ganser, 1964; Sorkhabi and Arita, 1997; Paudel and Arita, 2000).

Paleozoic orogenesis in the NW Himalaya of Pakistan.

2. GEOLOGICAL SETTING

The Himalayan mountain range, resulted from collision between the Indian and Eurasian plates, has been divided into four tectonic units. From the structural bottom to top, these tectonic units are: Sub-Himalaya, Lesser Himalaya, Higher Himalaya and Tethys Himalaya (Ganser, 1964; Le Fort, 1975; Hodges, 2000). The Lesser Himalaya is delimited by the Main Central Thrust (MCT) in the north and the Main Boundary Thrust (MBT) in the south. The Lesser Himalaya is primarily composed of igneous and metamorphic rocks of the Precambrian age. Igneous rocks are comprised of plutonic bodies which constitute MGC in the Mansehra area. Magmatic rocks of this complex occur as sub-concordant to discordant batholith that has intruded and surrounded by metapelites, psammites and quartzites of the Tanawal Formation (Fig. 2). The metasedimentary rocks have undergone Barrovian type regional metamorphism from greenschist to sillimanite-bearing amphibolites facies (Shams, 1971; Le Fort et al., 1980; Baig et al., 1989; Shah, 2009, Kohn, 2014). Field description of the MGC magmatic rocks is described below.

2.1. The Mansehra Granite

The MG is the most important member of the MGC Lesser Himalayan Granite Belt in Pakistan (Fig. 2). It is a two-mica, high-potash, medium to coarse-grained and porphyritic rock containing K-feldspar phenocrysts of variable size and amount. The matrix to phenocrysts ratio ranges from 70:30 to 95:05. Phenocrysts are eumorphic and commonly show Carlsbad twining. The groundmass is composed of K-feldspar, albite/plagioclase, quartz and biotite with subordinate muscovite; zircon, apatite, tourmaline, ilmenite and chlorite are accessory minerals. The granite shows parallel to sub-parallel arrangement of undeformed mica, quartz and K-feldspar phenocrysts, which is typical for flow-foliation (Fig. 3a) resulting from intrusion movements and superimposed flattening strain pertaining to the load of sedmentary sequence (Fernandez, 1983). The granite is generally undeformed and massive but intense shearing at local level has imparted mylonitic fabric in Susalgali, Darband and Jhargali areas where parallel arrangement of mica wrapping around deformed quartz and augen-shaped K-feldspar phenocrysts typifies solid-state strain (Fig. 3b). Ductile shear zones are superimposed on flow-foliation.

2.2. The Hakale Granite

The HG is a leucocratic laccolith elongated in the NE-SW direction, spreading over an area of 35 km^2 (Fig. 2). The rock is massive, medium to coarse-grained, non-porphyritic to rarely porphyritc. The Hakale Granite has weak to no flow-

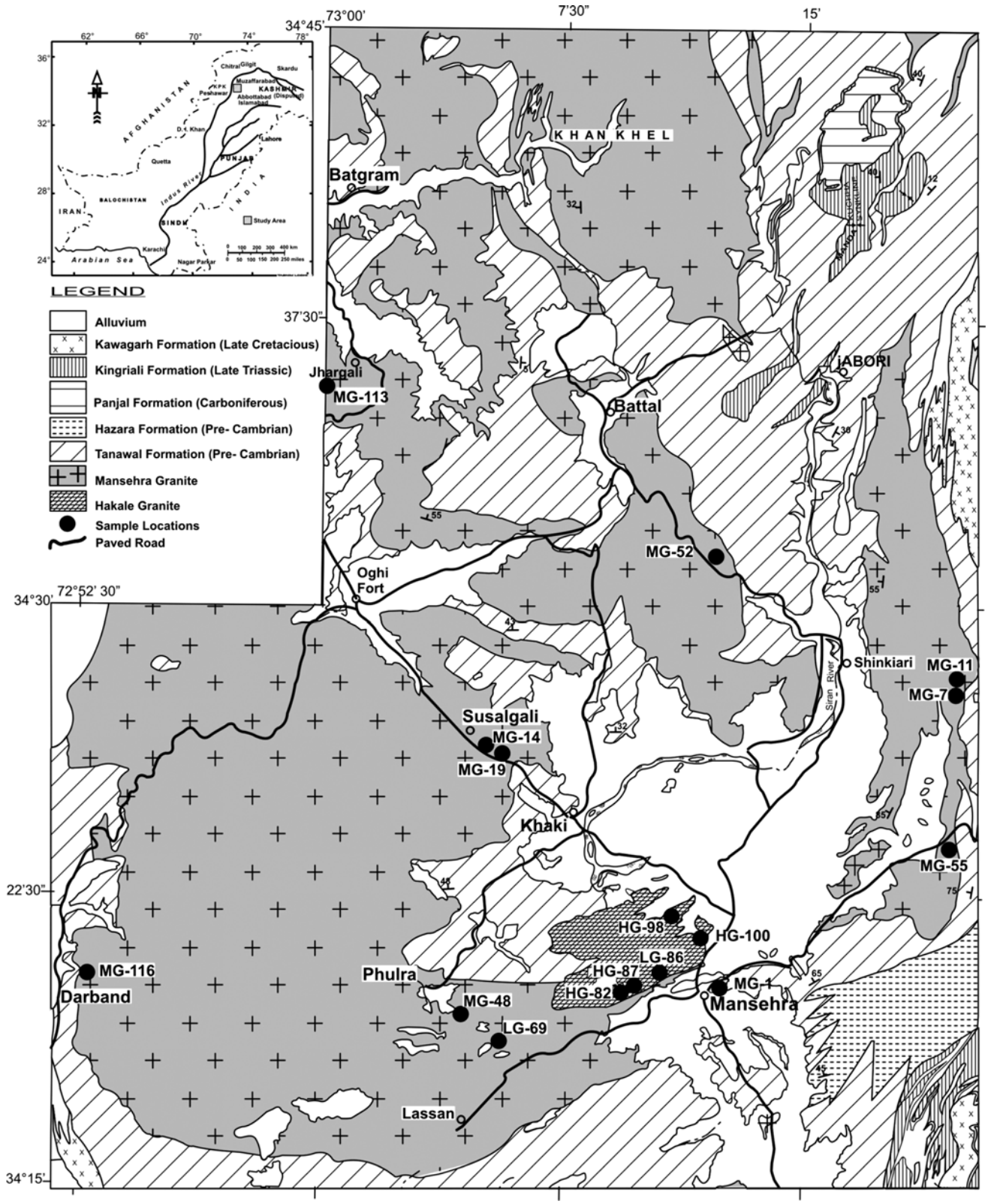

Fig. 2. Geological map of the Mansehra area (modified after Calkins et al., 1975) with location of dated samples taken for this study (see Table 1 for detail).

foliation. Tourmaline is ubiquitous. The matrix to phenocrysts ratio is 100:00 to 95:05. The HG has chilled contact with Mansehra Granite which is characterized by relatively fine-grained phenocrysts of the former (Fig. 3c). This contact

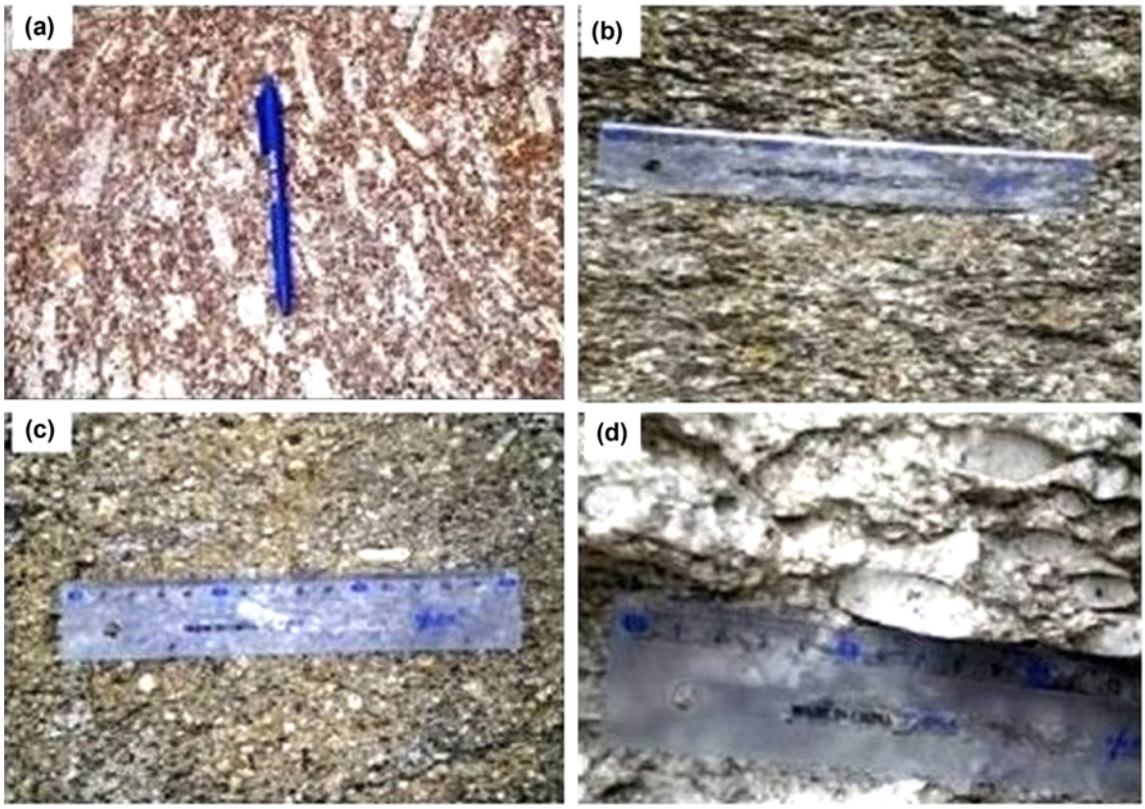

Fig. 3. (a) Massive Mansehra Granite showing flow-foliation of K-feldspar phenocrysts (sample location: N34°26′06″, E73°05′16″), (b) Gneissic Mansehra Granite (ruler is 15 cm long) (sample location: N34°38′56″, E72°59′42″), (c) Smaller size phenocrysts at the chilled margin of Mansehra and Hakale Granites (sample location:N34°20′07″, E73°11′13″), (d) Stretched and augen shaped K-feldspar phenocrysts in leucogranitic body near Mansehra (sample location: N34°19′54″, E73°07′53″).

shows that HG has intruded into the main body of MG and the country Tanawal Formation (Rehman, 1961; Shams, 1971).

2.3. Leucogranites

Leucocratic bodies of small extent are generally massive and rarely contain K-feldspar phenocrysts that may or may not define a flow-foliation. K-feldspar phenocrysts content varies from 3 to 6% with size ranging between 1 and 4 cm. The leucogranites have intrusive contacts with the MG. These leucogranites have been locally sheared (Fig. 3d).

2.4. Other Magmatic Bodies

Minor basic dykes, aplites and leucocratic bodies have intruded into the MG, HG and the Tanawal Formation (Shams, 1961; 1967; Ashraf, 1974). Dolerite dykes are up to 40 m thick and their length can be traced from few meters to 0.5 km. Aplites occur as small veins in granites and associated metasediments.

3. PETROGRAPHY

In this section, we present the general petrography of the MGC. Microcline, plagioclase, quartz, biotite and muscovite are the main minerals in Mansehra Granite (MG) and Hakale Granite (HG), whereas zircon, apatite, tourmaline, chlorite and ilmenite are accessories. The main differences in the MGC granitic bodies are:

3.1. Mansehra Granite

Mansehra Granite (MG) is the most widespread occurring magmatic body of the MGC. The MG contains microcline which is subhedral to anhedral, medium to coarse-grained and constitutes 30–40% of the granite. It is microperthitic and shows Carlsbad twinning (Fig. 4a). Alteration to sericite is common. Plagioclase forms 10–20% of the rock. It is fine to medium-grained, subhedral to anhedral, occasionally twinned and encloses muscovite. At places, myrmekites are developed between K-feldspar and plagioclase (Fig. 4b). Quartz is fine to medium-grained, subhedral to anhedral, variably strained grains showing undoluse extinction. Modal quartz content varies in the range of 35–40%. Grains are interlocked and exhibit mosaic texture. Strained and fractured quartz grains have sutured contacts. Fine-grained quartz bands associated with deformed muscovite and biotite flakes occur in shear zones.

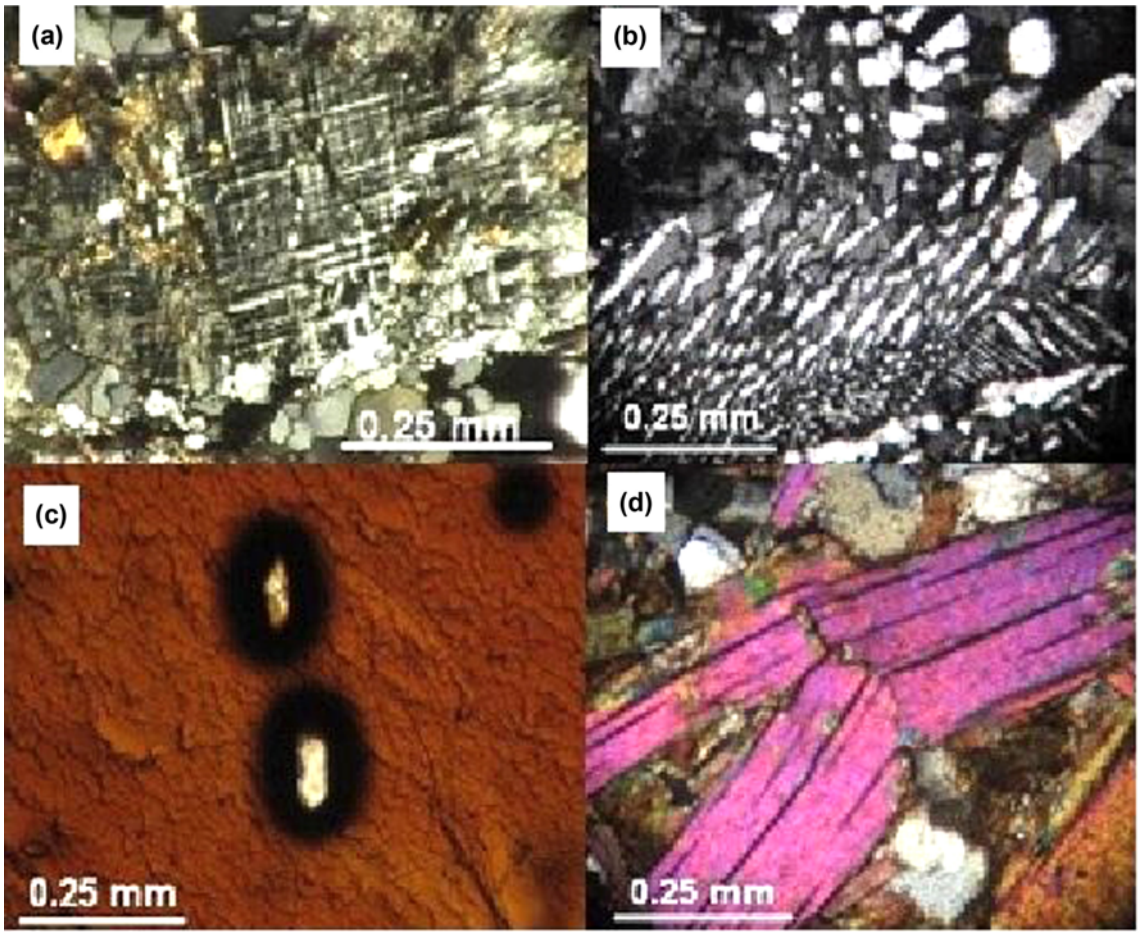

Fig. 4. (a) Cross-hatched, twinned microcline associated with quartz and biotite in Mansehra Granite, (b) Myrmekites in Hakale Granite, (c) Reddish-brown biotite flake encloses euhderal zircon crystals surrounded by dark haloes, (d) broken biotite flakes in Mansehra Granite.

Biotite constitutes 2–10% of the granite. It is strongly pleochroic with straw yellow to reddish brown colour, and occurs as randomly oriented subhedral lath. Biotite encloses quartz grains, prismatic apatite and ilmenite, and subhedral to euhedral zircon which is surrounded by dark halos (Fig. 4c). Biotite shows replacement by fine-grained muscovite.

Muscovite content is about 3–8%. Muscovite and biotite flakes can be stretched, while feldspar and quartz grains are fractured at places, which represent mild degree of deformation (Fig. 4d). Tourmaline (1–2%) occurs as subhedral to anhedral crystals. It is pleochroic from light yellow to deep brown and replaces biotite, muscovite and feldspar. Apatite is found as discrete euhedral to subhedral crystals (0.5%) in biotite. Rutile occurs as acicular crystals. Chlorite (0.5%) is witnessed as secondary mineral in few samples.

3.2. Hakale Granite

Hakale Granite (HG) is the second igneous body of the MGC, which is exposed in Mansehra area. The HG has microcline that is microperthitic, medium to coarse-grained and varies between 30 and 40% of the granite. Plagioclase is albite which constitutes 15–20% of the granite. It is medium-grained and shows well-developed polysynthetic twinning. Quartz forms 30–40% of the granite which generally shows moderate to strong strain extinction. Quartz grains have sutured contacts, and exhibit mild to intense marginal mylonization. Biotite abundance of the Hakale Granite is in the range of 1–5%, whereas muscovite constitutes 3–7% of the granite. Tourmaline (1–5%) is subhedral to anhedral, showing yellow to dark brown pleochroism. Apatite (0.3%) is eumorphic and included in biotite. Zircon and ilmenite are 0.5 and 0.4%, respectively, whereas chlorite is present in traces.

3.3. Leucogranites

Major minerals of the leucogranites (LG) are microcline, albite, quartz and muscovite, whereas accessory minerals include zircon, tourmaline and chlorite. Leucogranites contain 45–60% modal albite which is the distinctive feature of these rocks. Microcline is microperthitic, subhedral to anhedral and varies in the range of 10–15%. Quartz constitutes 2–45% of the rock. Albite is partly replaced by fine-grained muscovite. Muscovite ranges from 1 to 7% of the rock. Euhe-

dral to subhedral zircon is enclosed in subhedral and dark brown biotite. Occasionally subhedral to anhedral, yellowish tourmaline is observed. Chlorite occurs in traces.

4. TECHNICAL AND ANALYTICAL PROCEDURES

For radiometric dating six representative samples of Mansehra Granite, Hakale Granite and leucogranites, each weighing 5–10 kg, were collected from Jhargali (E72°59′37″, N34°35′04″), Susalgali (E73°05′02″, N34°26′07″; E73°05′58″, N34°25′55″), Darband (E72°54′49″, N34°25′18″), Karkale (E73°10′07″, N34°20′17″) and Mansehra (E73°10′35″, N34°20′19″) areas. Locations of samples are given in Table 1 and in Figure 2. Rock samples were crushed and the material was passed through a Frantz magnetic separator to concentrate the non-magnetic fraction of minerals. Using methylene iodide the heavy fraction was separated and individual euhedral zircon crystals were hand-picked under binocular microscope.

The Cathodoluminescence (CL) Images study was carried out at the ETH, Switzerland. Euhedral zircon crystals of the MG, HG and LG were mounted by epoxy resin and polished to reveal internal structure of the zircon crystals through SEM.

Although zircon morphology can be observed under optical microscope but this technique does not reveal the internal structure of these crystals. Multiple textural zoning and growths can be deciphered through cathodoluminescence (CL) images of the zircon crystals (e.g., Hanchar and Rudnick, 1995; Varva et al., 1996). Hence, before in situ dating of the MGC, zircon, cathodoluminescence (CL) imaging was carried out to infer possible multiple textural growth relations within zircons to correctly interpret the obtained U-Pb dates.

U-Pb Zircon dating of MG from Jhargali was carried out with SHRIMP analysis, whereas, samples of MG, HG and LG from Susalgali, Darband, Karkale and Mansehra were analyzed with LA-ICP-MS technique. Cores and rims of the zircon crystals were targeted. The data were plotted in the Tera-Wasserburg (1972) Concordia diagrams to reveal inherited and intrusive age components.

U-Pb zircon dating was carried out at ETH, Zurich, Switzerland. The data obtained was processed by the method of Williams (1998). Common Pb corrections were made through measurements of $^{238}U/^{206}Pb$ and $^{207}Pb/^{206}Pb$ ratios proposed by Tera-Wasserburg (1972). The plots were used to determine concordant radiometric dates. The error ellips for each analyzed zircon crystals is given as 2σ in the Concordia diagrams. The upper and lower intercept ages and the concordant dates are presented at 95% confidence level (Ludwig, 2001).

For the determination of major and selected trace elements MG, HG and LG samples were crushed by using jaw crusher at Pakistan Council of Scientific and Industrial Research Laboratories Complex, Lahore. Crushed samples were carefully sorted, washed to remove dust particles and dried at 110 °C. Size of the crushed samples was further reduced by roll crusher, which was thoroughly cleaned after each sample to avoid contamination. The ground material was passed through sample splitter to get representative sample of each rock type. About 200 g of each sample was powdered in TEMA tungsten carbide grinding mill for chemical analysis. Major and trace elements contents were determined by X-ray Fluorescence (XRF) technique. For major elements fused lithium tetraborate discs were prepared following the method of Norish and Hutton (1969). For the determination of trace ele-

Table 1. Analyzed samples (plotted in Fig. 1) and their locations

Sample Number	Location	Rock Unit	Type
MG-1	N34°20′27″ E73°11′29″	Mansehra Granite	Massive
MG-7	N34°27′46″ E73°19′58″	Mansehra Granite	Massive
MG-11	N34°27′51″ E73°19′56″	Mansehra Granite	Massive
MG-14[a]	N34°26′07″ E73°05′02″	Mansehra Granite	Gneissic
MG-19[a]	N34°25′55″ E73°05′58″	Mansehra Granite	Gneissic
MG-44[a]	N34°25′18″ E72°54′49″	Mansehra Granite	Massive
MG-48	N34°19′07″ E73°04′47″	Mansehra Granite	Massive
MG-52	N34°31′08″ E73°12′06″	Mansehra Granite	Massive
MG-55	N34°23′51″ E73°19′17″	Mansehra Granite	Massive
MG-113[a]	N34°35′04″ E72°59′37″	Mansehra Granite	Gneissic
MG-116	N34°20′28″ E72°52′16″	Mansehra Granite	Gneissic
HG-82[a]	N34°20′17″ E73°10′07″	Hakale Granite	Massive
HG-87	N34°20′27″ E73°10′49″	Hakale Granite	Massive
HG-98	N34°22′00″ E73°11′14″	Hakale Granite	Massive
HG-100	N34°21′39″ E73°11′43″	Hakale Granite	Massive
LG-69	N34°18′36″ E73°05′45″	Leucogranite	Massive
LG-86[a]	N34°20′19″ E73°10′35″	Leucogranite	Massive

[a]Sample used for U-Pb zircon dating.

ments, pressed pellets were prepared by using fusion machine (Phoenix 4000 VFD, Australia). The analyses of pellets were conducted by using wavelength-dispersive XRF spectrometer (Pw 4400/24 Axios, PANalytical, Netherlands). Necessary corrections for matrix effect and the spectral overlapping were employed. Some of the major elements (Na, K) and trace elements (Cr, Co, Ni and Cu) were determined by using a duly standardized Atomic Absorption Spectrometer (Thermo Scientific iCE 3000 Series, UK).

Moisture contents of the powdered samples were removed at 110 °C and loss on Ignition (LOI) was determined by taking 5.0 g of each sample in a platinum crucible and heating at 1050 °C for 6–8 hours in muffle furnace. FeO was determined by standard titration method following Furman (1962).

5. GEOCHEMISTRY

Sampling sites for geochronology and geochemistry are plotted on Figure 2. A total eleven samples of Mansehra Granite (MG-1, 7, 11, 14, 19, 44, 48, 52, 55, 113 and 116), four samples of Hakale Granite (HG-82, 87, 98 and 100) and two of leucogranite (LG-69 and 86) were analyzed. The major oxides and trace elements contents in each type of granite are presented in Table 2.

The MGC plutonic rocks have high SiO_2 contents, mean values ranged between 70.75 and 74.93%. Al_2O_3 varies from 14.79 to 16.26%. Mansehra Granite and Hakale Granite contain relatively higher K_2O contents (4.05–5.05%) as compared with the leucogranites (1.01%). In contarary the leucogranites show higher Na_2O values (6.50%) relative to the Mansehra Granite and Hakale Granite (2.90–3.34%). All these rocks have lower CaO (0.94%), MgO (0.80%) and Na_2O (3.44%) as compared with K_2O (4.35%) contents. A/CNK values are in the range of 1.52–2.25 which indicate peraluminous nature of the MGC magmatic bodies (Table 2). The magmatic bodies show enrichment of Ba (mean 217 ppm) and Rb (mean 233 ppm) relative to Sr (mean 48 ppm). Rb/Sr and Rb/Ba ratio varies in the range of 2.40–5.35 and 0.59–1.92, respectively. The chemical data and modal mineralogical composition of the MGC plutonic bodies were plotted in QAP and AFM

Table 2. Major and trace elements in percentage and ppm of Mansehra Granite (MG), Hakale Granite (HG) and leucogranites (LG)

Major Oxides	MG-1	MG-7	MG-11	MG-14	MG-19	MG-44	MG-48	MG-52	MG-55	MG-113	MG-116	HG-82	HG-87	HG-98	HG-100	LG-69	LG-86
SiO_2	70.01	69.81	71.67	71.69	71.86	71.15	70.16	72.03	68.4	71.58	69.45	72.06	74.23	74.68	74.94	74.85	71.00
Al_2O_3	14.43	15.40	15.38	15.14	15.05	17.02	15.04	15.02	17.01	15.65	16.35	15.02	14.86	14.66	14.59	15.35	17.16
Na_2O	3.19	3.16	2.83	2.75	2.47	1.34	3.48	2.78	3.84	4.04	3.64	2.74	2.75	4.29	3.20	6.35	6.65
MgO	1.52	0.81	0.95	0.54	0.59	1.50	1.17	0.92	0.97	0.10	0.58	0.54	0.74	0.48	0.16	0.25	1.79
CaO	1.24	1.18	1.20	1.01	1.19	1.04	1.47	1.37	1.40	0.41	0.83	1.01	1.06	0.71	0.56	0.14	0.08
K_2O	5.09	5.19	4.91	5.29	5.35	4.32	4.71	4.59	4.78	5.40	5.86	5.28	4.52	2.48	4.23	1.11	0.91
Fe_2O_3	0.71	1.67	0.46	1.17	0.28	0.96	0.89	0.58	0.74	0.42	0.34	1.17	0.04	0.63	0.94	0.01	0.09
FeO	2.11	1.32	1.21	1.05	1.93	0.89	1.72	1.70	1.72	1.03	1.63	0.81	0.91	0.76	0.56	0.41	0.68
MnO	0.09	0.09	0.08	0.14	0.10	0.07	0.05	0.09	0.10	0.02	0.04	0.10	0.06	0.07	0.06	0.02	0.01
P_2O_5	0.31	0.22	0.19	0.17	0.10	0.07	0.24	0.18	0.24	0.20	0.30	0.17	0.18	0.25	0.28	0.06	0.01
TiO_2	0.83	0.49	0.54	0.34	0.36	0.92	0.58	0.44	0.44	0.45	0.27	0.33	0.42	0.16	0.13	0.18	0.51
LOI	0.47	0.65	0.56	0.69	0.68	0.62	0.43	0.28	0.33	0.69	0.69	0.77	0.17	0.83	0.34	1.24	1.10
SUM	100	99.99	99.98	99.98	99.96	99.90	99.94	99.98	99.97	99.99	99.98	100	99.94	100	99.99	99.97	99.99
A/CNK	1.52	1.62	1.72	1.67	1.67	2.21	1.56	1.72	1.70	1.77	1.58	1.66	1.78	1.96	1.83	2.02	2.25
Trace Elements																	
Cr	8	54	20	17	18	17	16	36	34	8	10	65	52	21	19	1	14
Co	6	14	4	12	3	6	9	7	6	7	4	9	4	8	8	8	1
Ni	8	13	5	20	3	5	10	10	7	1	1	18	8	13	3	1	6
Cu	14	39	10	77	65	44	17	17	13	1	7	18	8	14	64	1	5
Rb	254	254	238	258	189	187	289	253	220	190	348	264	243	232	422	82	35
Sr	63	60	67	55	66	78	54	64	45	7	38	63	54	45	19	21	13
Y	29	27	25	23	26	31	27	28	20	10	30	28	26	19	22	10	4
Zr	139	148	128	104	105	183	125	129	103	13	94	126	114	58	44	146	136
Nb	14	15	13	13	9	15	15	15	13	7	17	14	13	14	17	17	18
Sn	34	37	32	33	27	29	35	35	33	33	43	38	37	55	60	48	35
Ba	248	279	354	337	320	269	250	281	180	29	187	316	248	121	116	117	37
Rb/Sr	4.03	4.23	3.55	4.69	2.86	2.40	5.35	3.95	4.89	27.14	9.16	4.19	4.50	5.16	22.21	3.90	2.69
Rb/Ba	1.02	0.91	0.67	0.77	0.59	0.70	1.16	0.90	1.22	6.55	1.86	0.84	0.98	1.92	3.64	0.70	0.95

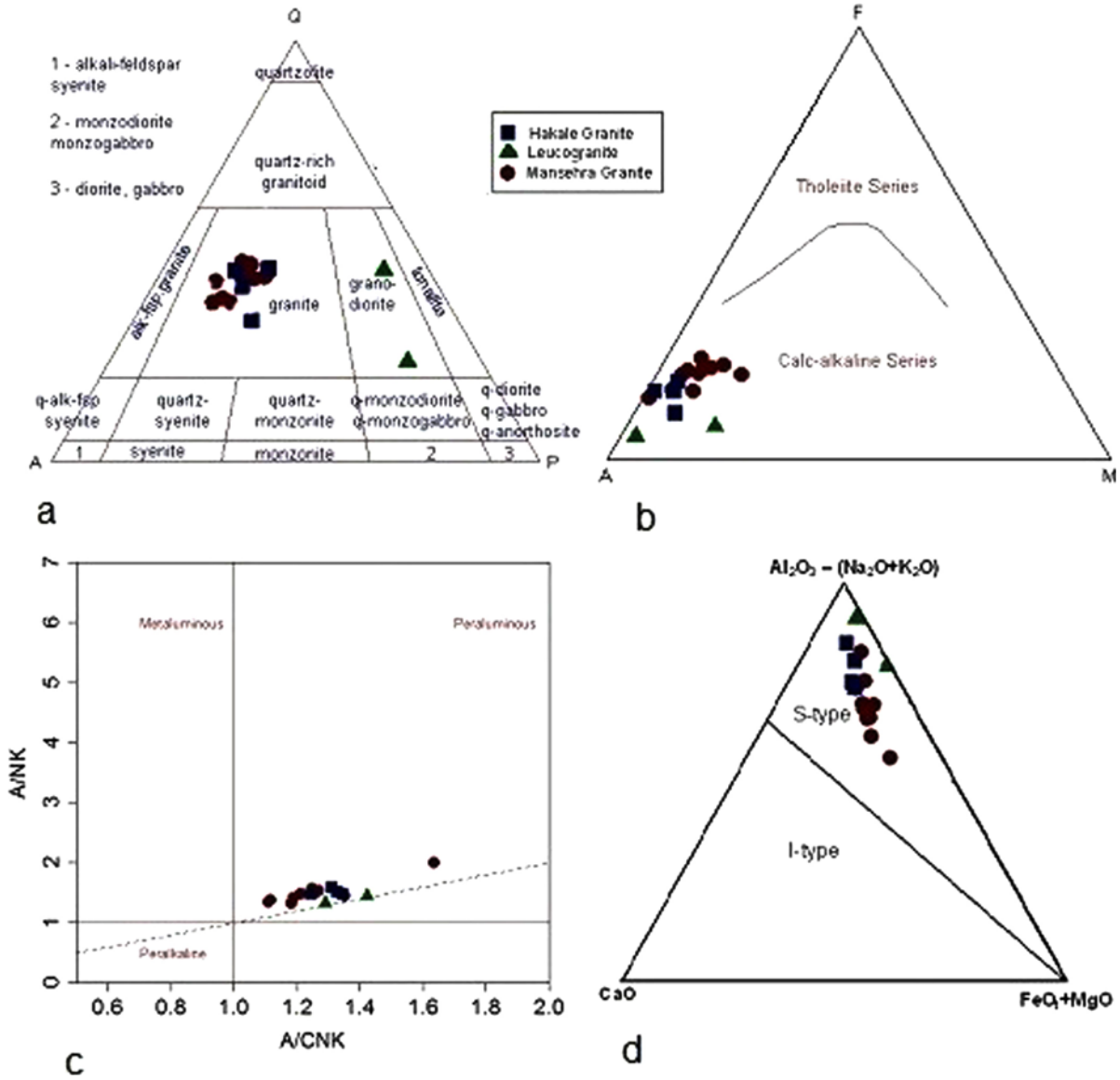

Fig. 5. Geochemical classification diagrams. (a) QAP (Streckeisen, 1974), (b) AFM diagram (Irvin and Baragar, 1971), (c) A/CNK-A/NK plot (Shand, 1943), (d) S-type granite classification diagram (Wang et al., 2013).

diagrams (Streckeisen, 1974; Irvin and Baragar, 1971) which placed these rocks in calc-alkaline, granite fields (Figs. 5a and b). Using the A/CNK plot (Shand, 1943) these granites are peraluminous (Fig. 5c). Plot of CaO, FeOt + MgO and Al_2O_3-(Na_2O + K_2O) in ternary diagram (Wang et al., 2013) indicates S-type trait of the MGC magmatic rocks (Fig. 5d). Chemical data of these plutonic rocks plot in syn-collision domain of R1-R2 geotectonic diagram (Batchelor and Bowden, 1985; Fig. 6).

6. U-Pb ZIRCON GEOCHRONOLOGY

Zircon crystals of the Mansehra Granite from Jhargali (sample MG-113) are euhedral which vary from 200 to 300 μm in length and 70–100 μm in width. About 70% of the zircon crystals have length/width (l/w) ratios in the range of 1–3. These crystals are nearly opaque, having off-white to yellowish white colour and contain reddish brown to dark grey inclusions with dark haloes due to radiation damage. A few (1–2%) transparent zircon crystals were also observed. Zircon crystals from Jhargali do not have core-rim structure (Fig. 7).

Mansehra Granite from Susalgali and Darband (MG-14, MG-19 and MG-44), Hakale Granite from Karkale (HG-82) and Leucogranite from Mansehra (LG-86) reveal the occurrence of euhedral zircon. These vary in length between 5 and 150 μm and from 20 to 50 μm in width. Length to width ratio (l/w) 1–3 is common, wheras l/w in the range of 1–2 and 1–4 characterize few crystals. Zircon grains are either transparent or opaque under the microscope. The transparent population is comprised of 70–75% light brown and 15–20% reddish

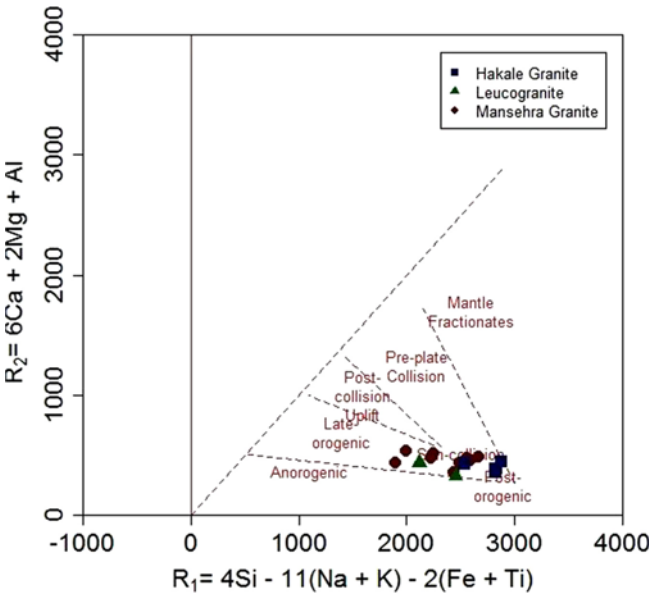

Fig. 6. Plot of chemical composition of selected samples of Mansehra Granite, Hakale Granite and leucogranites in R1-R2 tectonic discrimination diagram (Batchelor and Bowden, 1985).

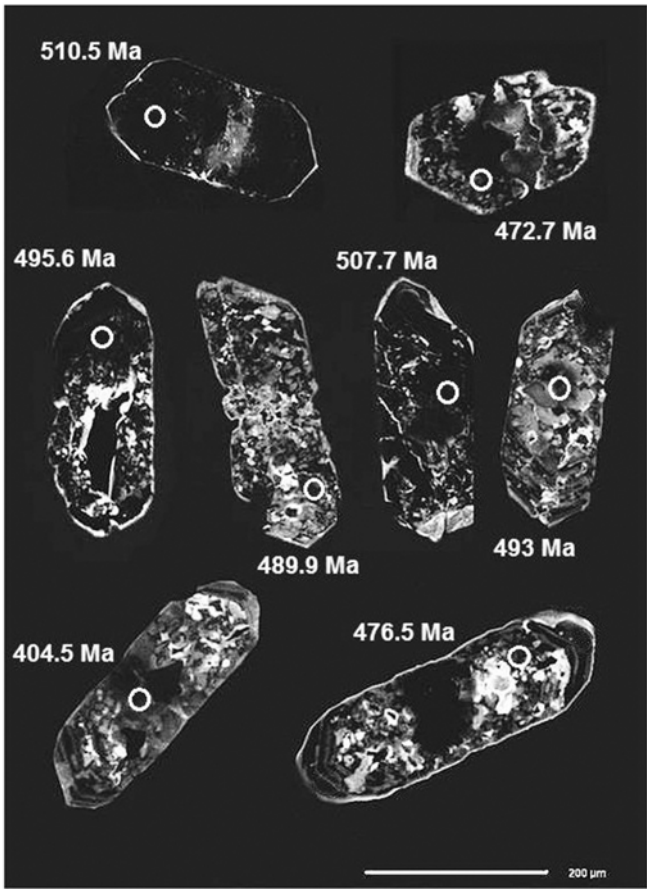

Fig. 7. Cathodoluminescence (CL) images of zircon from the Mansehra Granite of Jhargali (N34°35′04″, E72°59′37″).

brown grains, while the opaque component consists of 5–10% off-white (milky) and about 5% reddish-brown grains. The euhedral and transparent variety typifies a magmatic origin (Pupin, 1980). Zircon crystals from Susalgali, Darband, Karkale and Mansehra possess core–rim structures (Fig. 8). Undisturbed oscillatory zoning in some crystals indicates their magmatic affinity (Heuberger et al., 2007). Discordant overgrowth with oscillatory zoning suggests recrystallization during post-magmatic episodes (Corfu et al., 2003; Heuberger et al., 2007).

6.1. U-Pb Zircon Systematics

6.1.1. Sample MG-113 (E72°59′37″, N34°35′04″)

Mansehra Granite at Jhargali is a coarse-grained and gneissic rock with well-developed foliation and augen-shaped K-feldspar phenocrysts. About 90% of the zircon crystals are relatively opaque with dark haloes due to radiation damage. These crystals make a homogeneous population with very high U metamict zones and no inherited cores. Some domains are strongly altered.15 spots on 10 zircon crystals were analyzed with the SHRIMP technique (Table 3). The Tera-Wasserburg (1972) plot of the analytical data displays a concordant age at 490.1 ± 6.7 Ma and 491.3 ± 6.8 Ma with mean square weighted deviation (MSWD) 3.5 and 3.8 at 95% confidence level (c.l.). The intrusive age ranges between 477 ± 17 Ma and 479 ± 15 Ma (Figs. 9a and b). The average SHRIMP age of the Mansehra Granite is 478 ± 16 Ma.

6.1.2. Sample MG-14 (E73°05′02″, N34°26′07″)

Sample of the Mansehra Granite at Susalgali is medium-grained, porphyritic, highly gneissic, showing alignment of mica flakes along with stretched K-feldspar and deformed quartz crystals. 14 spots, including rim and cores, were targeted on 9 different zircon grains (Table 3) and Tera-Wasserburg diagrams (1972) of data are in Figures 10a and b. Inherited components have ages of 500, 580, 840–860, 1300 Ma with lower and upper intercepts age at 582 ± 120 Ma and 1513 ± 190 Ma, respectively. The Concordia isochrone reveals intrusion age of 477 ± 11 Ma at 95% c.l. with MSWD equal to 2.0 and probability at 0.14.

6.1.3. Sample MG-19 (E73°05′58″, N34°25′55″)

The Mansehra Granite collected in the Susalgali area is medium-grained, porphyritic and gneissic. The tectonic foliation is superimposed on flow-foliation. 15 spots on cores and rims of 11 zircon crystals were analyzed (results in Table 3). Measurements reveal inherited ages around 800–850 Ma and 985 Ma, while one discordant point yields $^{207}Pb/^{206}Pb$ age of 1.9 Ga. The lower and upper intercepts are at 650 ± 120 Ma and 1791 ± 260 Ma The Tera-Wasserburg isochrone indicates concordant age at 482.8 ± 2.3 Ma at 95% c.l, and MSWD = 0.93 (Figs. 10c and d).

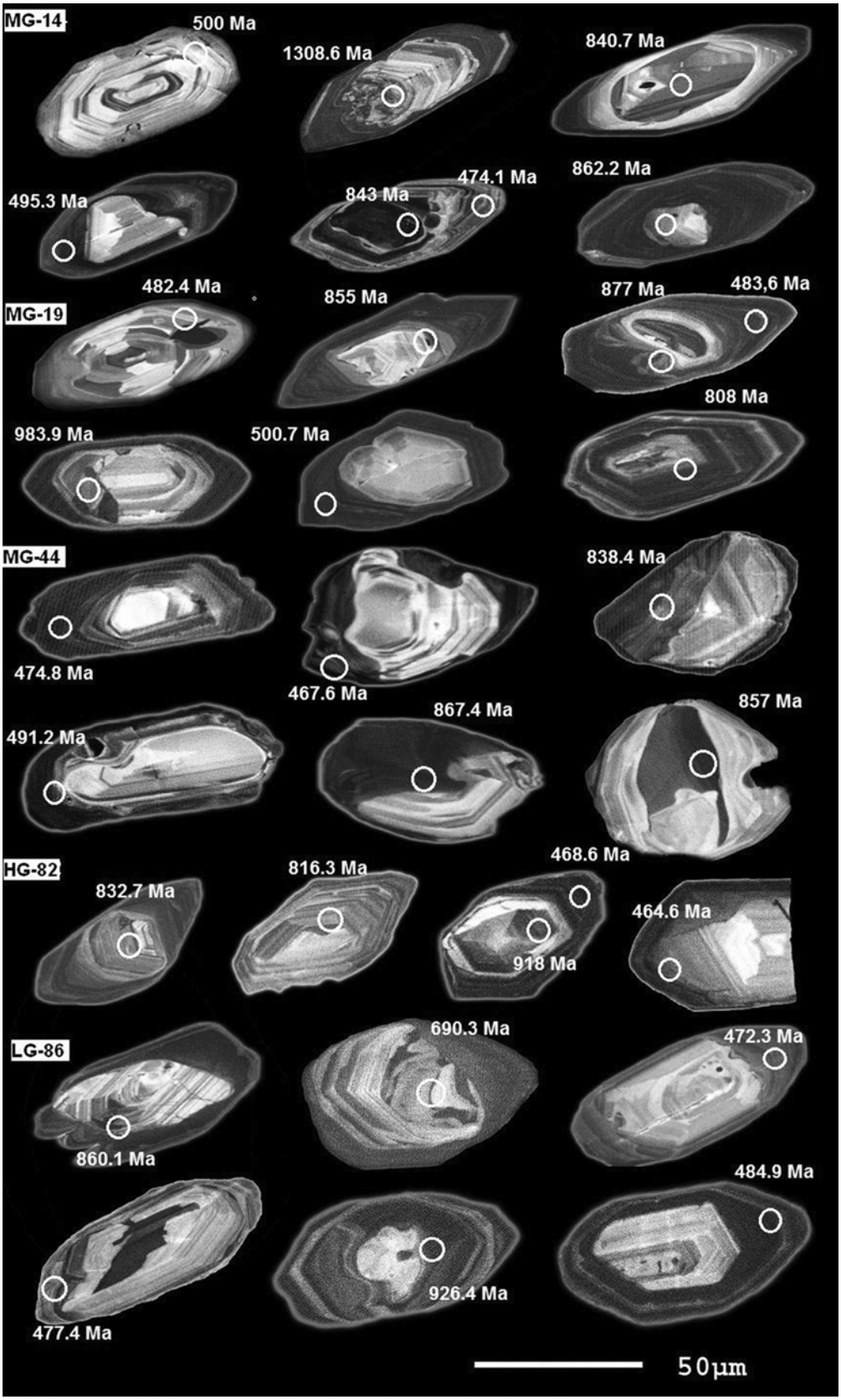

Fig. 8. Cathodoluminescence (CL) images of zircon from Mansehra Granite (MG) of Susalgali (N34°26′07″, E73°05′02″) and Darband (N34°25′55″, E73°05′58″), Hakale Granite (HG) of Karkala (N34°20′17″, E73°10′07″) and Leucogranites (LG) from Mansehra (N34°20′19″, E73° 10′35″).

Table 3. Analytical results of SHRIMP and LA-ICP-MS zircon U-Pb dating of Mansehra Granite, Hakale Granite and Leucogranite from Mansehra area

Spot	$^{206}Pb_c$ (%)	U (ppm)	Th (ppm)	$^{232}Th/^{238}U$	$^{206}Pb^*$ (ppm)	(1) $^{206}Pb/^{238}U$ Age (Ma)	(1) $^{207}Pb/^{206}Pb$ Age (Ma)	(1) $^{238}U/^{206}Pb^*$	±%	(1) $^{207}Pb^*/^{206}Pb^*$	±%	(1) $^{207}Pb^*/^{235}U$	±%	(1) $^{206}Pb^*/^{238}U$	±%	error
Mansehra Granite (MG-113)																
1.1	0.00	6397	10	0.00	453	510.5 ± 9.2	535 ± 19	12.13	1.9	0.05813	0.85	0.661	2.1	0.0824	1.9	.910
2.1	0.04	6667	13	0.00	440	476.5 ± 8.7	461 ± 20	13.04	1.9	0.05623	0.91	0.595	2.1	0.0767	1.9	.901
3.1	0.04	12266	35	0.00	864	507.7 ± 9.3	478 ± 16	12.20	1.9	0.05665	0.72	0.640	2.0	0.0819	1.9	.935
2.2	0.25	1533	5	0.00	85.5	404.5 ± 7.8	404 ± 59	15.44	2.0	0.05480	2.6	0.489	3.3	0.0648	2.0	.603
4.1	0.06	10151	22	0.00	719	510.5 ± 9.2	484 ± 19	12.13	1.9	0.05680	0.85	0.645	2.1	0.0824	1.9	.911
5.1	0.82	9587	211	0.02	632	472.7 ± 8.6	485 ± 35	13.14	1.9	0.05683	1.6	0.596	2.5	0.0761	1.9	.764
6.1	0.08	6447	11	0.00	450	503.2 ± 9.2	477 ± 25	12.32	1.9	0.05664	1.1	0.634	2.2	0.0812	1.9	.862
6.2	0.08	5390	11	0.00	353	472.6 ± 8.8	472 ± 24	13.14	1.9	0.05650	1.1	0.593	2.2	0.0761	1.9	.869
6.3	0.33	2096	7	0.00	108	374.7 ± 7.2	318 ± 69	16.71	2.0	0.05280	3.0	0.435	3.6	0.0599	2.0	.549
7.1	0.12	6941	17	0.00	477	495.6 ± 9.1	482 ± 22	12.51	1.9	0.05676	0.98	0.625	2.1	0.0799	1.9	.889
7.2	0.08	6677	13	0.00	454	490.6 ± 9.0	476 ± 25	12.65	1.9	0.05660	1.1	0.617	2.2	0.0791	1.9	.863
7.3	0.44	1569	5	0.00	93.5	430.3 ± 8.4	403 ± 75	14.48	2.0	0.05480	3.3	0.521	3.9	0.0690	2.0	.519
8.1	0.08	5349	9	0.00	363	489.9 ± 9.1	446 ± 26	12.67	1.9	0.05584	1.1	0.608	2.2	0.0789	1.9	.860
9.1	0.15	5424	10	0.00	371	493.0 ± 9.3	462 ± 30	12.58	2.0	0.05624	1.3	0.616	2.4	0.0795	2.0	.826
10.1	0.17	7011	30	0.00	476	489.9 ± 9.2	453 ± 26	12.66	2.0	0.05601	1.2	0.610	2.3	0.0790	2.0	.861

Zircon grain	Core/Rim	$^{206}Pb/^{238}U$		$^{207}Pb/^{235}U$		$^{207}Pb/^{206}Pb$		$^{206}Pb/^{238}U$		$^{207}Pb/^{235}U$		$^{207}Pb/^{206}Pb$	
		Ratio	R.S.D.	Ratio	R.S.D.	Ratio	R.S.D.	Age (Ma)	±2 S.D.	Age (Ma)	±2 S.D.	Age (Ma)	±2 S.D.
Mansehra Granite (MG-14)													
1	Core	0.2251	0.67%	2.7150	1.32%	0.08895	0.81%	1308.6	15.9	1332.6	19.6	1402	32
1	Rim	0.1206	0.73%	1.0844	1.78%	0.06593	1.60%	733.8	10.2	745.8	18.8	804	66
2	Rim	0.0763	0.66%	0.5823	1.15%	0.05588	0.84%	474.1	6.0	465.9	8.6	446	38
2	Core	0.1393	0.55%	1.2574	0.82%	0.06765	0.47%	840.7	8.6	826.7	9.3	856	20
3	Rim	0.0806	0.54%	0.5936	0.69%	0.05554	0.68%	500.0	5.2	473.2	5.2	432	30
4	Rim	0.0799	0.59%	0.5988	0.71%	0.05686	0.58%	495.3	5.6	476.4	5.4	484	26
5	Rim	0.0776	0.64%	0.6088	0.89%	0.05648	0.88%	481.9	6.0	482.8	6.8	470	40
5	Core, old	0.1431	0.67%	1.6931	1.51%	0.08562	0.90%	862.2	10.9	1006	19.3	1328	34
6	Core	0.1397	0.81%	1.3013	2.05%	0.06835	1.55%	843.0	12.7	846.3	23.6	878	64
7	Core	0.1721	0.66%	1.7119	1.17%	0.07424	0.86%	1023.6	12.5	1013	15.0	1046	34
7	Rim	0.0940	0.72%	0.7867	1.10%	0.06095	0.88%	579.3	8.0	589.3	9.8	636	38
8	Core	0.2602	0.79%	3.6309	2.21%	0.10295	1.08%	1491.0	20.9	1556.3	35.2	1678	40
8	Rim	0.0821	0.63%	0.6374	0.76%	0.05856	0.63%	508.6	6.1	500.7	6.0	550	28
10	Rim	0.0764	0.82%	0.5893	2.25%	0.05666	1.81%	474.8	7.5	470.4	17.0	478	80
Mansehra Granite (MG-19)													
1	Rim	0.0777	0.53%	0.6087	0.71%	0.05762	0.64%	482.4	4.9	482.7	5.5	514	28
3	Core, old	0.1418	0.62%	1.3211	1.16%	0.06848	0.80%	855.0	9.9	855.0	13.4	882	32
4	Core, old	0.1458	0.66%	1.3174	2.15%	0.06783	1.37%	877.3	10.8	853.4	24.9	862	56
4	Rim	0.0782	0.54%	0.6132	1.00%	0.05746	0.88%	485.6	5.1	485.6	7.7	508	40
5	Core, old	0.1335	0.62%	1.2689	1.33%	0.06848	1.24%	808.0	9.4	831.9	15.1	882	52
6	Core	0.0768	0.90%	0.5923	2.51%	0.05576	1.88%	476.8	8.3	472.4	18.9	442	84
6	Rim	0.0775	0.64%	0.6633	0.86%	0.06205	0.80%	481.3	6.0	516.6	7.0	676	34
7	Core, old	0.1333	0.81%	1.1727	3.47%	0.06482	1.59%	806.7	12.2	787.9	38.0	768	66
8	Core, old	0.3105	0.49%	5.0062	2.65%	0.11552	0.86%	1743.2	15.1	1820.4	44.8	1888	30

9	Core, old	0.1409	0.58%	1.2990	1.75%	0.06699	1.38%	849.7	9.2	845.3	20.1	836	56
9	Rim	0.0808	0.55%	0.6219	0.80%	0.05771	0.66%	500.7	5.3	491.0	6.2	518	28
10	Core, old	0.1649	0.56%	1.6404	1.43%	0.07184	1.15%	983.9	10.2	985.9	18.0	980	48
11	Core, old	0.1352	0.65%	1.2938	1.43%	0.06882	1.03%	817.3	9.9	843.0	16.4	892	42
11	Rim	0.1362	1.18%	1.3110	4.20%	0.06741	2.52%	823.4	18.2	850.5	48.4	850	106
12	Rim	0.0779	0.47%	0.6024	0.88%	0.05688	0.69%	483.6	4.4	478.7	6.7	486	32
Mansehra Granite (MG-44)													
1	Rim, old	0.1389	0.46%	1.3106	1.43%	0.06793	0.90%	838.4	7.3	850.4	16.4	866	38
2	Rim	0.0752	0.74%	0.5899	1.96%	0.05752	1.46%	467.6	6.7	470.8	14.8	510	64
5	Core, old	0.0792	0.70%	0.6328	1.28%	0.05819	0.92%	491.2	6.6	497.8	10.1	536	40
6	Rim	0.0764	0.43%	0.6037	1.10%	0.05649	0.82%	474.8	4.0	479.6	8.4	470	36
8	Core, old	0.2132	0.48%	2.5038	0.99%	0.08483	0.57%	1245.7	11.0	1273.1	14.3	1310	22
8	Core, old	0.1422	0.70%	1.3957	1.78%	0.07099	1.05%	857.0	11.3	887.1	21.0	956	44
10	Core	0.0761	0.77%	0.5845	2.72%	0.05654	2.12%	472.6	7.0	467.3	20.3	472	94
11	Core	0.1440	0.81%	1.3834	2.75%	0.06992	1.52%	867.4	13.1	881.9	32.5	924	62
Hakale Granite (HG-82)													
1	Rim, old	0.1530	0.63%	1.4761	2.41%	0.07111	1.72%	918.0	10.7	920.6	29.2	960	70
1	Core, old	0.1533	0.97%	1.3833	3.14%	0.06962	1.78%	919.5	16.6	881.8	37.0	916	72
3	Core, old	0.1350	0.37%	1.2352	1.14%	0.06651	0.65%	816.3	5.7	816.7	12.8	822	28
4	Core, old	0.2824	0.58%	3.7759	1.66%	0.09929	0.89%	1603.3	16.4	1587.6	26.7	1610	32
5	Core, old	0.2903	0.35%	4.2656	0.98%	0.10684	0.50%	1642.8	10.1	1686.7	16.1	1746	18
5	Rim	0.0758	0.34%	0.5862	0.83%	0.05719	0.77%	470.9	3.1	468.4	6.2	498	34
6	Core, old	0.2360	0.47%	2.8380	1.23%	0.08976	0.59%	1365.8	11.6	1365.6	18.4	1420	22
6	Rim	0.0747	0.34%	0.5861	0.74%	0.05703	0.62%	464.3	3.0	468.4	5.6	492	28
7	Core, old	0.1379	0.61%	1.3668	2.70%	0.07262	1.35%	832.7	9.6	874.8	31.6	1002	56
8	Core, old	0.1344	0.55%	1.2439	1.59%	0.06719	0.99%	812.9	8.5	820.6	17.8	842	42
9	Core	0.0744	0.76%	0.5685	2.86%	0.05564	2.00%	462.8	6.8	457.0	21.0	438	90
9	Rim	0.0747	0.48%	0.5895	0.92%	0.05693	0.80%	464.6	4.3	470.5	7.0	488	36
10	Rim	0.0747	0.44%	0.6029	1.30%	0.05802	1.09%	464.6	4.0	479.0	9.9	530	48
10	Rim	0.0753	0.44%	0.5922	0.88%	0.05695	0.83%	468.1	4.0	472.3	6.7	488	36
Leucogranites (LG-86)													
1	Core, old	0.2379	0.74%	3.0368	2.28%	0.08996	1.30%	1376	18.2	1416.9	34.8	1424	50
1	Rim	0.0775	0.58%	0.6164	1.41%	0.05810	1.11%	481.1	5.4	487.6	10.9	532	48
2	Rim	0.0760	0.49%	0.5880	1.13%	0.05606	0.90%	472.3	4.5	469.6	8.5	454	40
3	Core, old	0.1545	0.47%	1.5361	1.04%	0.07210	0.75%	926.4	8.1	945.0	12.8	988	32
3	Rim	0.0761	0.40%	0.5936	0.84%	0.05636	0.67%	472.9	3.6	473.1	6.4	466	30
4	Core, old	0.1427	0.59%	1.3509	1.85%	0.06865	1.36%	860.1	9.5	868.0	21.6	888	56
5	Core, old	0.1456	0.50%	1.3509	0.81%	0.06792	0.71%	876.0	8.3	868.0	9.4	866	30
6	Core, old	0.1130	0.47%	0.9841	1.15%	0.06320	0.78%	690.3	6.2	695.7	11.6	714	32
6	Rim	0.0767	0.38%	0.5789	0.74%	0.05588	0.53%	476.7	3.5	463.7	5.5	446	24
7	Rim	0.0781	0.48%	0.6032	0.88%	0.05589	0.82%	484.9	4.5	479.3	6.7	448	38
8	Core, old	0.1400	0.80%	1.2967	2.27%	0.06778	1.68%	844.6	12.6	844.2	26.0	860	70
9	Core, old	0.1413	0.59%	1.3314	1.71%	0.06769	1.18%	852.1	9.5	859.5	19.8	858	48
9	Rim	0.0769	0.43%	0.5872	0.74%	0.05626	0.62%	477.4	4.0	469.1	5.6	462	28

Errors are 1-sigma; Pb and Pb^* indicate the common and radiogenic portions, respectively.
Error in Standard calibration is 0.60%.
(1) Common Pb corrected using measured ^{204}Pb.

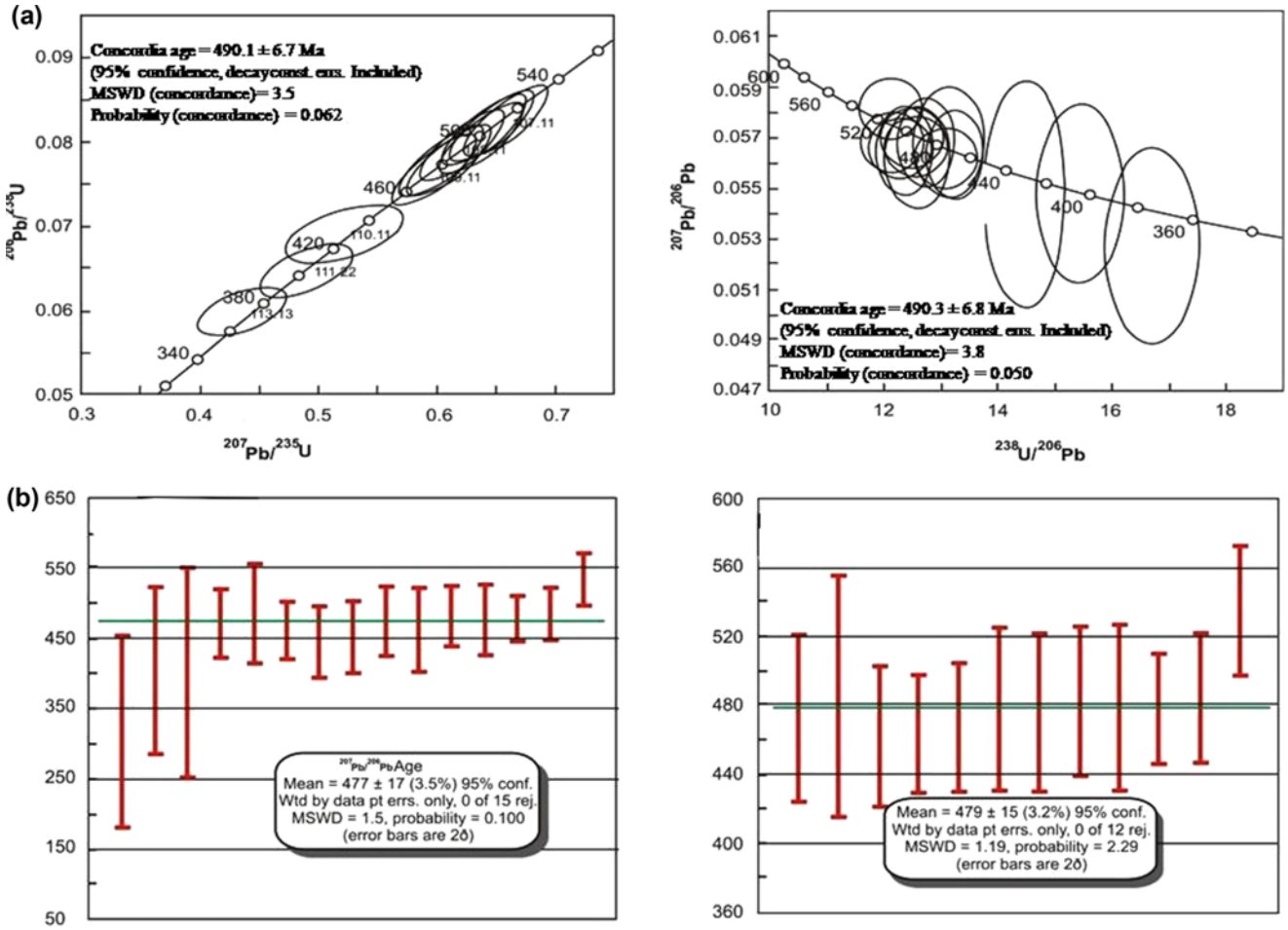

Fig. 9. (a) Concordia diagrams showing (a) intrusive and (b) mean intrusive ages of the Mansehra Granite.

6.1.4. Sample MG-44 (E72°54′49″, N34°25′18″)

The Mansehra Granite at Darband is medium to coarse-grained, porphyritic, having K-feldspar phenocrysts along with poorly-developed flow-foliation. 7 zircon crystals were targeted by 8 spots (Table 3). The Tera-Wasserburg plot of the data exhibits an inherited component at 840–870 Ma. Lower and upper intercepts indicate ages at 523 ± 130 Ma and 1234 ± 180 Ma, respectively. Three rim ages yield the concordant $^{206}Pb/^{238}U$ age of 472.8 ± 8.7 Ma at 95% c.l., MSWD = 1.7 (Figs. 10e and f).

Mean age of the Mansehra Granite of Susalgali and Darband is 478 ± 12 Ma. The upper intercept at 1234 ± 180 Ma indicate the age of older magmatic events.

6.1.5. Sample HG-82 (E73°10′07″, N34°20′17″)

This sample of Hakale Granite is medium to coarse-grained, sub-porphyritic and contains K-feldspar phenocrysts. 9 zircon crystals were analyzed by 14 spots (Table 3). They yield inherited segments at 820–830, 920 Ma, 1.3 Ga and 1.6–1.7 Ga. Lower and upper intercepts of these components yield an age of 589 ± 150 Ma and 1549 ± 180 Ma, respectively, which indicate ages of older magmatic occurrences. The Tera-Wasserburg Concordia diagram revealed 466.5 ± 3.3 Ma from cluster of six rim ages with MSWD = 2.7 at 95% c.l. (Figs. 11a and b).

6.1.6. Sample LG-86 (E73°10′35″, N34°20′19″)

The leucogranite sample collected near Mansehra city is massive and non-foliated. 13 spots were analyzed on 9 zircon crystals by targeting the cores and rims (Table 3). The data plotted on Tera-Wasserburg diagram indicates inherited components at 690, 850–870 and 930 Ma, with lower and upper intercepts at 581 ± 120 Ma and 1315 ± 210 Ma, respectively. Six rim ages cluster around 478 Ma and concordant age of the leucogranite is 475.7 ± 3.9 Ma with MSWD = 2.4, at 95% c.l (Figs. 12a and b). Whereas, lower and upper intercepts ages reveal the dates of pre-intrusive magmatic episodes recorded in the zircon of the granite protolith.

7. DISCUSSION

The MGC magmatic rocks are calc-alkaline, peraluminous S-type granitoids which have >1.1 A/CNK value. Lower mean Na_2O and CaO contents relative to K_2O, enrichment

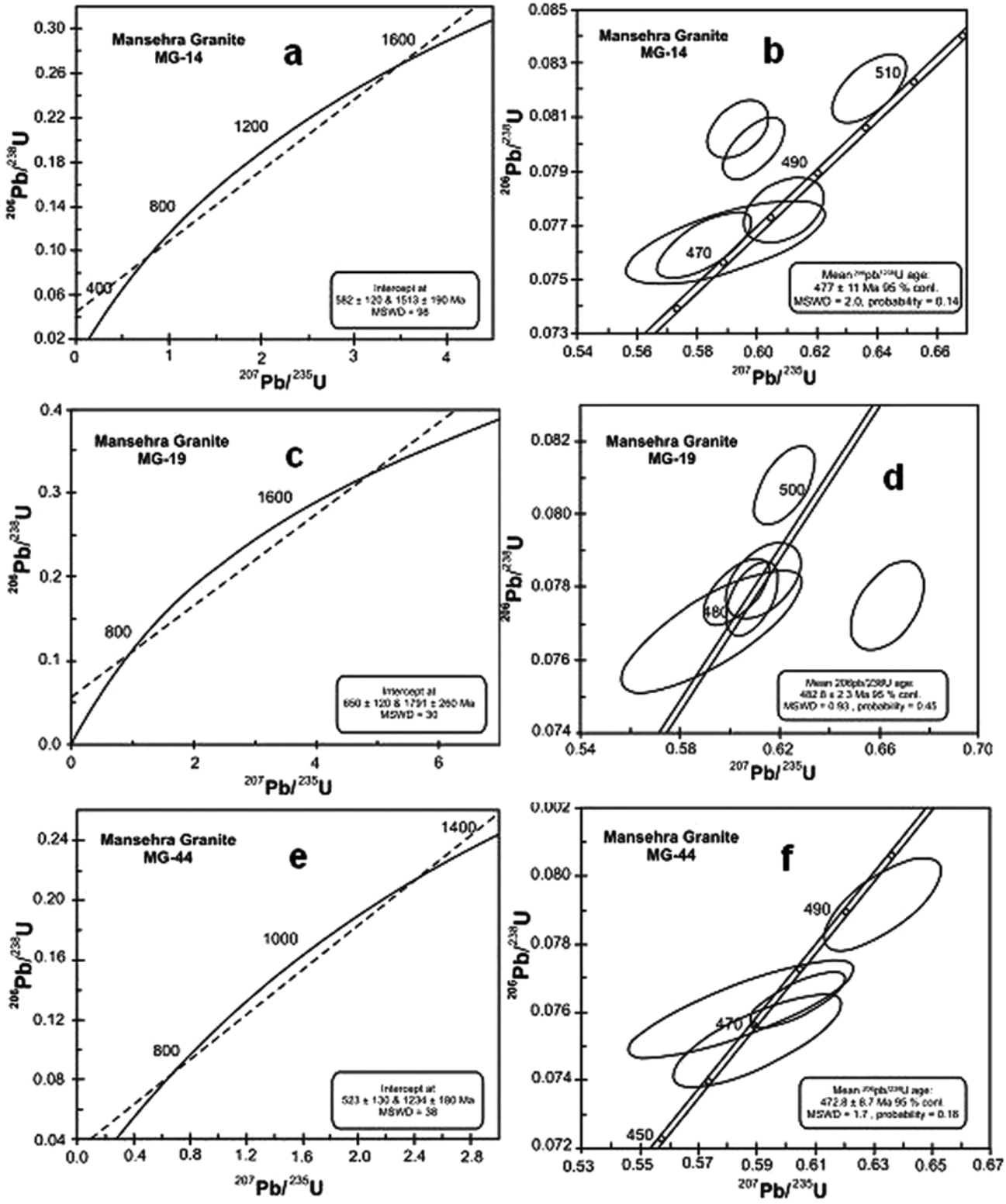

Fig. 10. Concordia diagrams presenting inherited (a, c, and e) and intrusive age components (b, d, and f) of the Mansehra Granite (samples: MG-14, 19, and 44).

of Ba and Rb as compared with Sr along with Rb/Ba and Rb/Sr ratio (0.59–1.92 and >0.25) indicate S-type traits and pelitic source of the MGC plutonic rocks as proposed by other workers in similar cases (Haak et al., 1982; Miller, 1985; Chappell and White, 1974; 1992; Williamson et al., 1997; Jung et al., 2000).

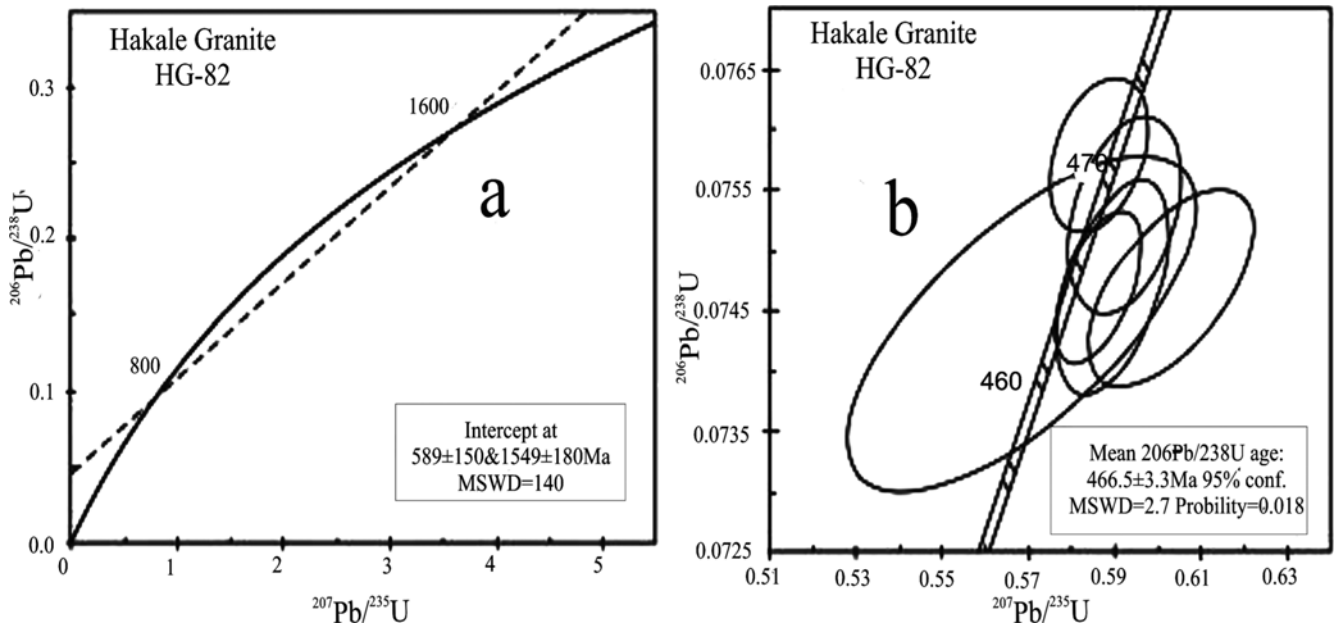

Fig. 11. Concordia diagrams indicating (a) inherited and (b) intrusive age components of the Hakale Granite (sample: HG-82).

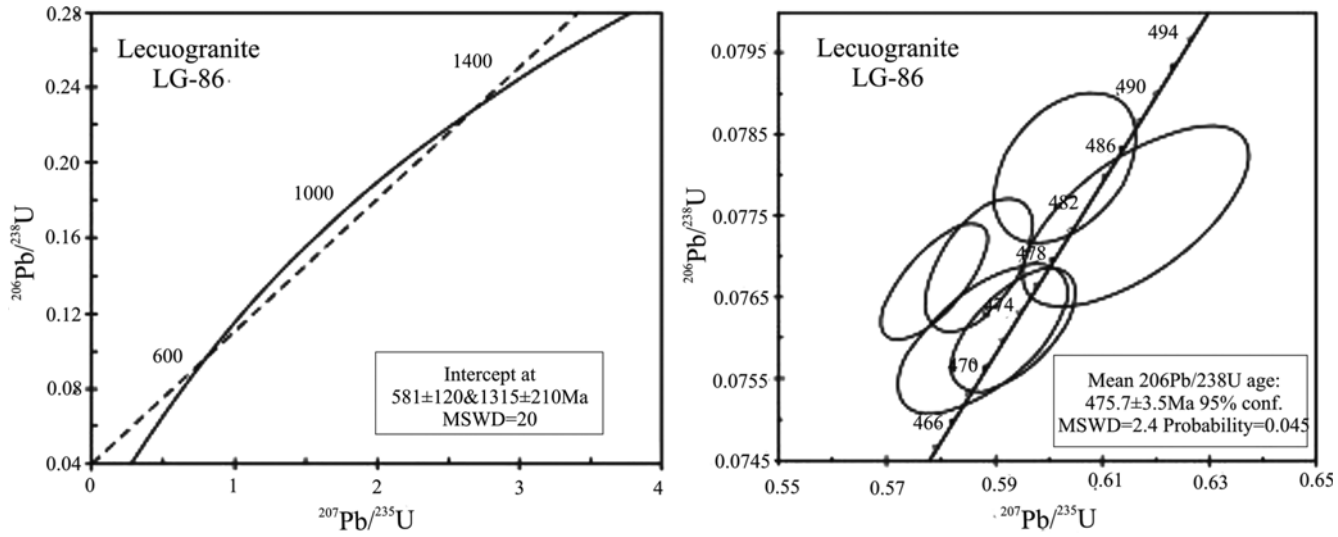

Fig. 12. Concordia diagrams presenting (a) inherited and (b) intrusive age segments of the leucogranite (sample: LG-86).

Interpreted U-Pb intrusive ages of the Mansehra Granite, leucogranites and Hakale Granite are 478, 475 and 466 Ma, respectively. These new dates are significantly different from the previously determined ages of MG at 79, 83 Ma (Shams, 1967), 215 Ma (Maluski and Matte, 1984), 516 ± 16 Ma (Le Fort et al., 1980) and HG 165 Ma (Shams, 1967), whereas radiometric date of leucogranite was not reported prior to this study. Lower U-Pb age of the Hakale Granite (466 Ma) is consistent with field evidence of chilled margin which indicates that this granite is intrusive into the main body of Mansehra Granite.

The older $^{206}Pb/^{238}U$ age components of ca. 1900–1300, 880–800, 985–920 and 690–500 Ma are interpreted as inherited grains which most likely represent magmatic events experienced by zircon of the granite protolith revealed by discordant overgrowths in CL images of the MGC plutonic rocks. These inherited ages suggest that detrital zircon grains of the MGC magmatic bodies may have been derived from plutonic, and or basement rocks of Gondwana affinity. The U-Pb zircon age peaks at ca. 980, 800 Ma and 700–500 Ma have also been reported from Lesser Himalayan granites (Lie and Liang, 2010).

U-Pb zircon dates (ca. 478–466 Ma) of the MGC magmatic rocks are consistent with ca. 480–500 Ma Rb/Sr and U-Pb zircon ages of other magmatic complexes and gneisses emplaced in the Lesser Himalaya to the east in India (Jaeger

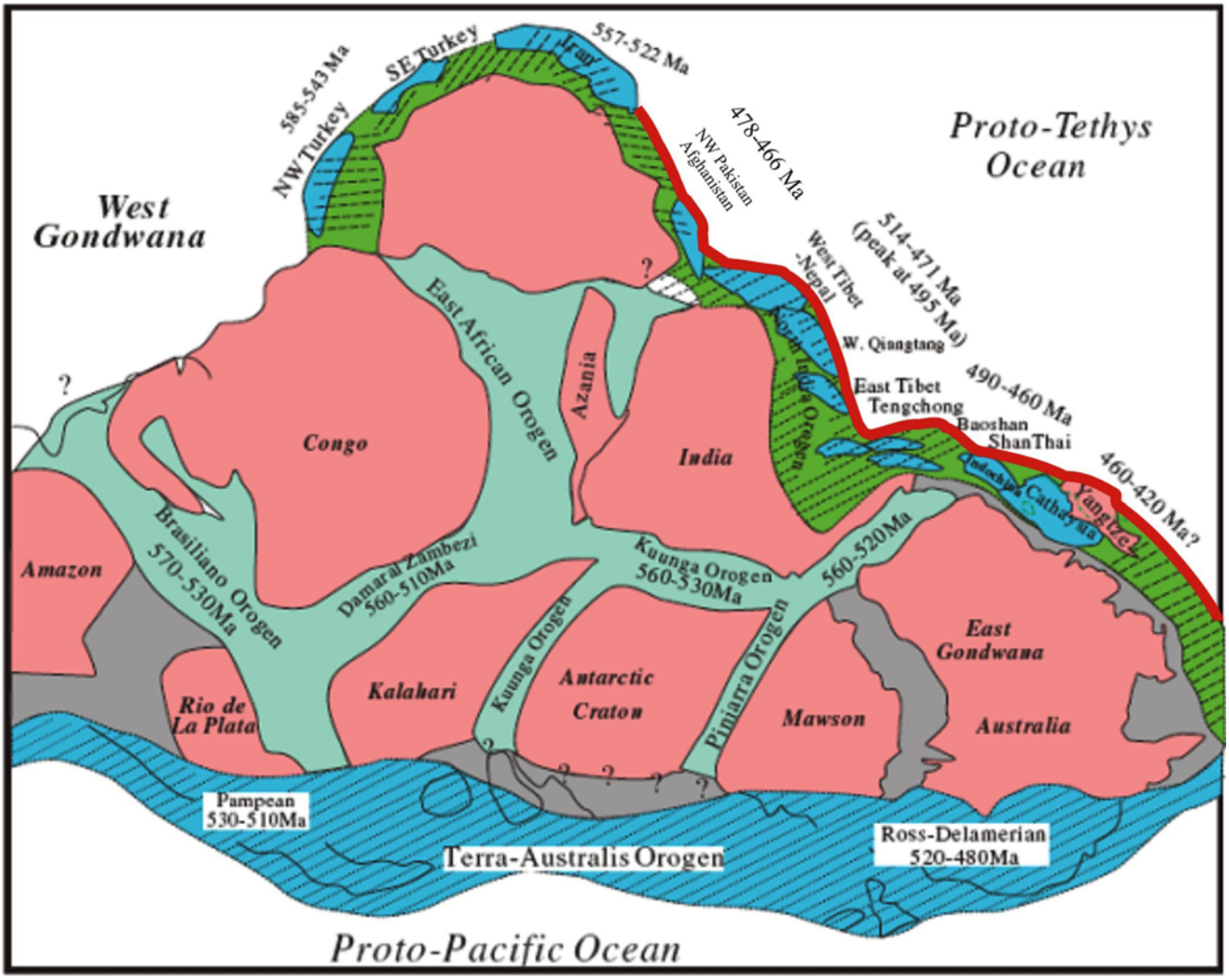

Fig. 13. Shows the age data, listed in Table 4, of early Paleozoic granitic rocks from China (SW Yunnan) to Turkey. Red line indicates the impact of Cambro-Ordovician orogeny along the eastern margin of northern Gondwana (modified after Wang et al., 2013).

et al., 1971; Ferrara et al., 1983; Trivedi et al., 1984; Le Fort et al., 1986; Hodges et al., 1996; DeCelles et al., 1998, 2000; Miller et al., 2001; Wang et al., 2013). Radiometric age data of plutonic rocks along the northern margins of east Gondwana is presented in Table 4. These ages also correspond with ca. 492–460 Ma U-Pb zircon dates of the corrundum normative and peraluminous S-type granites of SW Yunnan, China emplaced along the eastern margin of Gondwana. U-Pb zircon ages of the MGC at ca. 478–466 Ma suggest late Cambrian to middle Ordovician plutonism in the Mansehra area, NW Hmalaya of Pakistan. Geochronological and field evidence revealed the occurrence of Cambrian to early Ordovician felsic magmatism and coeval Barrovian type metamorphism in NW India, Nepal, Tibet, China (e.g., DeCelles et al., 2004; Xu et al., 2005; Cawood et al., 2007; Zhu et al., 2012; Wang et al., 2013) and NW Himalaya of Pakistan. In many parts of the Himalaya Cambrian and Ordovician stratigraphic sequences are separated by an angular unconformity (e.g., Le Fort et al., 1994; Hughes, 2002; Zhou et al., 2004; Myrow et al., 2006a, 2006b). In NW India, Nepal and south Tibet the Ordovician conglomerates/arkosic sandstone overlies the fine-grained marine sediments (e.g., Kumar et al., 1978; Stocklin, 1980; Myrow et al., 2006a, 2006b). An angular unconformity between Ordovician basal conglomerates and Cambrian–lower Ordovician sediments was recorded in China (Wang, 2000). Likewise in Himalayan tectonostrigraphic basin of northern Pakistan the Ordovician basal conglomerates of Misri Banda quartzite unconformably overly the Cambrian sequence of Ambar Formation (Shah, 2009), which indicate an early Paleozoic orogenesis in the NW Himalaya. Geochronological and field evidence demarcate the occurrence of a regional-level orogenic event in the Himalaya that extend from SW Yunnan (China) up to al least NW Hiamlaya, Pakistan through Tibet, Nepal and India along the northern margin of east Gondwana (Fig. 13). This Cambro-Ordovician felsic plutonism has affinity with an Andean-type thermotectonic

Table 4. Radiometric dates of plutonic rocks along the eastern and northern Gondwana (modified after Miller et al., 2001 and Wang et al., 2013)

Location	Lithology	Method	Age (Ma)	References
Gemlik, Pontides, NW Turkey	Metagranite	Zircon U-Pb	585	Okay et al. (2008)
Pamukova, Pontides, NW Turkey	Metagranite	Zircon Pb/Pb	543	Okay et al. (2008)
Dogruyol, Bitlis, SE Turkey	Peraluminous metagranite	Zircon U-Pb	572	Ustaömer et al. (2012)
Saltanich Mountain, South and East Zanjan, Central Iran	Foliated biotite granite	Zircon U-Pb	544	Hassanzadeh et al. (2008)
	Leucogranite	Zircon U-Pb	567	
	Beige leucogranite	Zircon U-Pb	559	
Kuh-e Molhedou, Central Iran	Foliated leucogranite	Zircon U-Pb	534	
Kuh-e Sefid Sang, Central Iran	Biotite–garnet granite	Zircon U-Pb	522	
SW Langarud, Central Itan	Pink biotite granite	Zircon U-Pb	551	Lam (2002)
Mansehra, Northern Pakistan	Mansehra Granite	Zircon U-Pb	478	This study
Mansehra, Northern Pakistan	Hakale Granite	Zircon U-Pb	466	This study
Mansehra, Northern Pakistan	Leucogranite	Zircon U-Pb	475	This study
Tso-Morari, NW India	Granite	Zircon U-Pb	479	Girard and Bussy (1999)
Rupshu, Ldakh	Granite	Zircon U-Pb	483	Girard and Bussy (1999)
Tsu Morari, Ladakh	Granite	Zircon U-Pb	479	Girard and Bussy (1999)
Tsu Morari, Ladakh	Gneiss	Zircon U-Pb	479	Girard and Bussy (1999)
Kangan, Zanskar	Granite	Rb-Sr/U-Pb	480	Trivedi (1990)
Mandu Khola, far-west Nepal	Granite	Zircon U-Pb	473	Gehrels et al. (2006b)
Mandu Khola, far-west Nepal	Granite	Zircon U-Pb	484	Gehrels et al. (2006b)
Ruwa, far-west Nepal	Granite	Zircon U-Pb	474	Gehrels et al. (2006a)
Ruwa, far-west Nepal	Granite	Zircon U-Pb	484	Gehrels et al. (2006a)
Ruwa, far-west Nepal	Granitic dike	Zircon U-Pb	474	Gehrels et al. (2006a)
Bhimphedi, far-west Nepal	Granite	Zircon U-Pb	476	Gehrels et al. (2006b)
Agra, far-west Nepal	Granite	Zircon U-Pb	480	Gehrels et al. (2006b)
Palung, Nepal	Granite	Rb-Sr/U-Pb	486	Trivedi (1990)
Palung, Nepal	Granite	Zircon U-Pb	470	Schärer and Allègre (1983)
Simchar	Granite	Zircon U-Pb	471	Johnson et al. (2001)
Kathmandu	Granite	Zircon U-Pb	477	Cawood et al. (2007)
Kathmandu	Granite	Zircon U-Pb	478	Cawood et al. (2007)
Dadeldhura	Granite	Zircon U-Pb	478	DeCelles et al. (2000)
Namche Barwa	Granet-bearing gneiss	Zircon U-Pb	490	Zhang et al. (2008)
Namche Barwa (Pai)	Garnet-, mica-bearing gneiss	Zircon U-Pb	493	Zhang et al. (2008)
Namche Barwa	Granitic gneiss	Zircon U-Pb	490	Zhang et al. (2008)
Amdo basement	Granitic gneiss	Zircon U-Pb	468	Guynn et al. (2012)
Amdo basement	Granodioritic gneiss	Zircon U-Pb	483	Guynn et al. (2012)
Amdo basement	Granitic gneiss	Zircon U-Pb	498	Guynn et al. (2012)
Amdo basement	Granitic gneiss	Zircon U-Pb	487	Guynn et al. (2012)
Central Lhasa terrane	Metarhyolite	Zircon U-Pb	491	Zhu et al. (2012)
Central Lhasa terrane	Metarhyolite	Zircon U-Pb	492	Zhu et al. (2012)
Gaoligong (Tengchong)	Leucogranite	Zircon U-Pb	485	Wang et al. (2013)
Gaoligong (Tengchong)	Gneissoid granite	Zircon U-Pb	488	Wang et al. (2013)
Pingda (Baoshan)	Granite	Zircon U-Pb	472	Chen et al. (2007)
Pingda (Baoshan)	Granite	Zircon U-Pb	466	Chen et al. (2007)
Pingda (Baoshan)	Monogranite	Zircon U-Pb	473	Wang et al. (2013)
Ximeng (ShanThai)	Leucogranite	Zircon U-Pb	463	Wang et al. (2013)
Ximeng (ShanThai)	Gneissoid granite	Zircon U-Pb	460	Wang et al. (2013)

event associated with proto-Tethyn subduction at ca. 490 Ma along the northern margin of Gondwana (e.g., Miller et al., 2001; Cawood et al., 2007; Zhu et al., 2012). The MGC magmatic bodies of ca. 478–466 Ma possess comparable radiometric dates with SW Yunnan, China ca. 488–460, Tibet 492–468, Nepal 493–470 and India 483–479 Ma which suggests Cambro-Ordovician felsic magmatism in NW Himalaya of Pakistan. The new crystallization ages of the MGC magmatic bodies at ca. 478–466 Ma demarcate continuation of the regional-level Cambro-Ordovicain thermotectonic envent (Bhimphidian Orogeny of Cawood et al., 2007) along the northern margin of east Gondwana. In view of the U-Pb zircon ages and field evidences, we propose that MGC plutonic rocks, like other Himalayan granites, are the product of Cambro-Ordovician orogenic episode along the northern margin of east Gondwana (Fig. 13). However, the age component at ca. 690–500 Ma recorded in the zircon of the MGC plutonic rocks might have affinity with the Pan-African orogeny which has been superimposed by a relatively younger Cambro-Ordovician magmatic event along the northern margin of east Gondwana. Ca. 700–500 Ma peak has also been documented from granitoids intruded in the Lesser Himalaya (Lie and Liang, 2010) defining the imprints of Pan-African thermotectonic episode. Granites of ca. 567–522 and 585–543 Ma have been reported from central Iran and Turkey along northen and western margins of Gondwana. We infer that the Paleozoic orogenesis commenced from SW China up to NW Pakistan and beyond that granitoids of Pan-African affinity were intruded along northern and western margins of Gondwana (Fig. 13).

Peraluminous S-type granites, formed from metasedimentary rocks, are the product of continental-continental collision (e.g., Wang et al., 2012a, 2012b). The peraluminous Mandi granite (India) of ca. 496 ± 14 Ma and bimodal volcanic rocks of Lhasa Block (Tibet) at ca. 492 Ma (late-Cambrian) are associated with convergent margin setting (e.g., Miller et al., 2001; Zhu et al., 2012). The MGC magmatic rocks show affinity with continental-continental margin (Fig. 6) similar to the peraluminous S-type granites of the Himalaya. Magma of these rocks was crystallized during deformational phase of the convergent regime which is manifested by the occurrence of myrmekites, marginal mylonization, parallel arrangement of mica flakes and microfractured quartz in the MGC plutonic bodies. The synthesis of the geochemical and geochronological data revealed that MGC magmatic rocks are associated with the early Paleozoic accretionary orogenesis of continental-continental settings.

8. CONCLUSION

Geochemical signatures revealed that MGC magmatic rocks are calc-alkaline, peraluminous S-type grantoids. U-Pb zircon dates of the Mansehra Granite, leucogranite and Hakale Granite at ca. 478, 475 and 466 Ma represent the intrsusive ages of these rocks. The age segments of ca. 1900–1300, 985–920, 880–800 and 690–500 Ma indicate dates of magmatic/melting events experienced by zircon inherited from the granite protolith. The new intrusive ages (ca. 478–466 Ma) are comparable to radiometric dates of the granites and gneisses present in the Lesser Himalaya to the east, in India. These rocks are most likely the product of Cambro-Ordovician compressional event (e.g., Cawood et al., 2007; Zhu et al., 2012) along the northern margin of east Gondwana. The age data indicates that the Andean-type Cambro-Ordovician thermotectonic event extends from SW China up to NW Himalaya of Pakistan and beyond that granitic rocks of Pan African orogeny were found in central Iran and Turkey along northern and western margin of Gondwana.

ACKNOWLEDGMENTS: We are highly grateful to Prof. Urs Schaltegger, Alexey Ulianov and Othmar Müntener for extending generous help regarding CL imaging and LA ICP-MS analysis for U-Pb zircon systematics. We are thankful to Dr. Izhar Ul Haque Khan for extending analytical facilities. Special recognition goes to my students Mr. Ahmed Humanyun Imtiaz, Hafiz Asif Saleem and Nasar Sahi for their assistance during field sampling. Dr. Shahid Tufail Sheikh, Head Mineral and Metallurgy Research Centre, PCSIR Laboratories Complex, Lahore is highly appreciated for providing sample preparation facilities.

REFERENCES

Ashraf, M., 1974, Geology and Petrology of Acid Minor bodied from Mansehra and Batgram area, Hazara district, Pakistan. Geological Bulletin of the Punjab University, 11, 81–88.

Ashraf, M. and Chaudhry, M.N., 1976a, Geology and classification of Acid Minor bodies of Mansehra and Batgram area, Hazara division, Pakistan. Geological Bulletin of the Punjab University, 12, 1–16.

Ashraf, M. and Chaudhry, M.N., 1976b, The geochemistry and petrogenesis of albitites from Mansehra and Batgram area, Hazara district, Pakistan. Geological Bulletin of the Punjab University, 13, 65–85.

Auden, J.B., 1932, On the age of certain Himalayan granites. Records of Geological Survey of India, 66, 461–471.

Baig, M.S., Snee, L.W., and La Fortune, R.J., 1989, Timing of the Pre-Himalayan organic events in the Northwestern Himalaya: $^{40}Ar/^{39}Ar$ constraints. Kashmir Journal of Geology, 6–7, 29–40.

Batchelor, RA. and Bowden, P., 1985, Petrogenetic interpretation of granitoid rock series using multicationic parameters. Chemical Geology, 48, 43–55.

Calkins, J.A., Offield, T.W., Abdullah, S.K., and Ali, S.T., 1975, Geology of the southern Himalaya in Hazara, Pakistan and Adjoining Areas. Geological Survey Professional Paper, 716-C, C1–C29.

Cawood, P.A., Johnson, M.R.W., and Nemchin, A.A., 2007, Early Paleozoic orogenesis along the Indian margin of Gondwana: Tectonic response to Gondwana assembly. Earth and Science Planetary Letters, 255, 70–84.

Chappell, B.W. and White, A.J.R., 1974, Two contrasting granite types. Pacific Geology, 8, 173–174.

Chappell, B.W. and White, A.J.R., 1992, I-Type and S-Type granites in the Lachlan Fold Belt. Transactions of the Royal Society of Edinburgh: Earth Sciences, 83, 1–26.

Chen, F.K., Li, X.H., Wang, X.L., Li, Q.L., and Siebel, W., 2007, Zir-

con age and Nd-Hf isotopic composition of the Yunnan Tethyan belt, southwestern China. International Journal of Earth Sciences, 96, 1179–1194.

Corfu, F., Hanchar, J.M., Hoskin, P.W.O., and Kinny, P., 2003, Atlas of zircon textures. In: Hanchar, J.M. and Hoskin, P.W.O. (eds.), Zircon. Review in Mineralogy and Geochemistry, 53, p. 469–500.

DeCelles, P.G., Gehrels, G.E., Quade, J., Ojha, T.P., Kapp, P.A., and Upreti, B.N., 1998, Neogene foreland basin deposits, erosional unroofing, and the kinematic history of the Himalayan fold-thrust belt, western Nepal. Geological Society of America Bulletin, 110, 2–21.

DeCelles, P.G., Gehrels, G.E., Quade, J., LaReau, B., and Spurlin, M., 2000, Tectonic implications of U-Pb zircon ages of the Himalayan Orogenic belt in Nepal. Science, 288, 497–499.

DeCelles, P.G., Gehrels, G.E., Najman, Y., Martin, A.J., Carter, A., and Garzanti, E., 2004, Detrital geochronology and geochemistry of Cretaceous–Early Miocene strata of Nepal: implications for timing and diachroneity of initial Himalayan orogenesis. Earth and Planetary Science Letters, 227, 313–330.

Fernandez, A., 1983, Strain analysis of typical granite of the Lesser Himalayan Cordierite Granite Belt: The Mansehra pluton, northern Pakistan. In: Shams, F.A. (ed.), Granites of Himalayas, Karakoram and Hindukush. Institute of Geology, University of the Punjab, Lahore, p. 183–199.

Ferrara, G., Lombardo, B., and Tonarini, S., 1983, Rb/Sr geochronology of granites and gneisses from the Mount Everest region, Nepal Himalaya. Geologische Rundschau, 72, 119–136.

Furman, N.H., 1962, Standard methods of chemical analysis. D. Van Nostrand Co., Inc. Princeton, 129 p.

Ganser, A., 1964, Geology of the Himalayas. Wiley Interscience, London, 289 p.

Gehrels, G.E., DeCelles, P.G., Ojha, T.P., and Upreti, B.N., 2006a, Geological and U-Pb geochronological evidence for early Paleozoic tectonism in the Dadeldhura thrust sheet, far-west Nepal Himalaya. Journal of Asian Earth Sciences, 28, 385–408.

Gehrels, G.E., Decelles, P.G., Ojha, T.P., and Upreti, B.N., 2006b, Geologic and U-Th-Pb geochronologic evidence for early Paleozoic tectonismin the Kathmandu thrust sheet, central Nepal Himalaya. Geological Society of America Bulletin, 118, 185–198.

Girard, M. and Bussy, F., 1999, Late Pan-Africanmagmatismin the Himalaya: newgeochronological and geochemical data from the Ordovician Tso Morari metagranites (Ladakh, NW India). Schweizerische Mineralogische und Petrographische Mitteilungen, 79, 399–418.

Griesbach, C.L., 1893, Notes on the Central Himalaya. Records of Geological Survey of India, 26, 19–25.

Guynn, J., Kapp, P., Gehrels, G.E., and Ding, L., 2012, U-Pb geochronology of basement rocks in central Tibet and paleogeographic implications. Journal of Asian Earth Sciences, 43, 23–50.

Haak, U., Hoefs, J., and Gohn, E., 1982, Constraints on the origin of Damaran granites by Rb/Sr and $\delta^{18}O$ data. Contributions to Mineralogy and Petrology, 79, 279–289.

Hancher, J.M. and Rudnick, R., 1995, Revealing hien structures: the application of Cathodoluminescence and back-scattered electron imaging to dating zircon from lower crustal xenoliths. Lithos, 36, 289–303.

Hassanzadeh, J., Stockli, D.F., Horton, B.K., Axen, G.J., Stockli, L.D., Grove, M., Schmitt, A.K., and Walker, J.D., 2008, U-Pb zircon geochronology of late Neoproterozoic–Early Cambrian granitoids in Iran: implications for paleogeography, magmatism, and exhumation history of Iranian basement. Tectonophysics, 451, 71–96.

Hayden, H.H., 1913, Notes on the relationship of the Himalayas and the Indo-gangetic plain and the Indian Peninsula. Records of Geological Survey of India, 43, 138–167.

Heuberger, S., Schaltegger, U., Burg, J.P., Villa, I.M., Frank, M., Dawood, H., Hussain, S., and Zachi, A., 2007, Age and isotopic constraints on magmatism along the Karakuram-Kohistan Suture Zone, NW Pakistan: evidence for subduction and continued convergence after India-Asian collision. Swiss Journal of Geoscience, 100, 85–107.

Hodges, K.V., Parrish, R.R., and Searle, M.P., 1996, Tectonic evolution of the Central Annapura Range, Nepalese Himalaya. Tectonics, 15, 1264–1291.

Hodges, K.V., 2000, Tectonics of the Himalaya and southern Tibet from two perspectives. Geological Society of America Bulleton, 112, 324–350.

Hughes, N.C., 2002, Late Middle Cambrian trace fossils from the Lejopyge armata horizon, Zanskar Valley, India, and the use of Precambrian/Cambrian isochronostratigraphy in the Indian subcontinent. Special Papers in Palaeontology, 67, 135–151.

Irvin, T.M. and Baragar, W.R., 1971, A guide to the chemical classification of common volcanic rocks. Canadian Journal of Earth Sciences, 8, 523–548.

Jaeger, F., Bhandari, A.K., and Bhanot, V.B., 1971, Rb-Sr age determinations on biotite and whole rock samples from the Mandi and Chor granites, Himachal Pradesh, India. Eclogae Geologicae Helvetiae, 64, 521–527.

Johnson, M.R.W., Oliver, G.J.H., Parrish, R.R., and Johnson, S.P., 2001, Synthrusting metamorphism, cooling and erosion of the Himalayan Kathmandu complex, Nepal. Tectonics, 20, 394–415.

Jung, S., Hoernes, S., and Mezger, K., 2000, Geochronology and petrogenesis of Pan-African syn-tectonic S-type and post-tectonic A-type granite (Namibia) – products of melting of crustal sources, fractional crystallization and wall-rock contaminant. Lithos, 50, 259–287.

Kohn, M.J, 2014, Himalayan metamorphism and its tectonic implications. Annual Review of Earth and Planetary Sciences, 42, 381–419.

Kumar, R., Shah, A.N., and Bingham, D.K., 1978, Positive evidence of a Precambrian tectonic phase in central Nepal, Himalaya. Journal of the Geological Society of India, 19, 519–522.

Lam, P.J., 2002, Geology, geochronology, and thermochronology of the Alam Kuh area, central Alborz Mountains, northern Iran. M.S. thesis, University of California, Los Angeles, 135 p.

Le Fort, P., 1975, Himalayas: the collided range-Pre-sent knowledge of the continental arc. American Journal of Science, 275-A, 1–44.

Le Fort, P., Debon, F., and Sonet, J., 1980, The "Lesser Himalayan" Cordeirite Granite Belt. Typology and Age of the Pluton of Mansehra (Pakistan). Proceedings of International Committee on Geodynamics, Group 6 Meeting, Peshawar, Nov. 23–29, 179.

Le Fort, P., Debon, F., Pecher, A., Sonet, J., and Vidal, P., 1986, The 500 Ma magmatic event in Alpine southern Asia, a thermal episode at Gondwana scale. Sciences de la Terre Memories, 47, 191–209.

Le Fort, P., Tongiorgi, M., and Gaetani, M., 1994, Discovery of a crystalline basement and Early Ordovician marine transgression in the Karakorum mountain range, Pakistan. Geology, 22, 941–944.

Lie, X. and Liang, S., 2010, Pre-Devonian tectonic evolution of the eastern south China Block: geochronological evidence from detrital zircon. Science China. Earth Science, 53, 1427–1444.

Ludwig, K.R., 2001, Isoplot/Ex version 2.49. A geochronological toolkit for Microsoft Excel. Berkeley Geochronological Center Special Publication la.

Maluski, H.F. and Matte, P., 1984, Ages of alpine tectonomorphic events in the north-western Himalaya (northern Pakistan) by $^{40}Ar/Ar^{39}$ method. Tectonics, 3, 1–18.

McMahon, C.A., 1884, Microscopic structures of some Himalayan granites and gneissose granites. Records of Geological Survey of India, 17, 53–73.

Miller, C.F., 1985, Are strong peraluminous magmas derived from pelitic sedimentary sources? Geology, 93, 673–689.

Miller, C., Thoni, M., Frank, W., Grasemann, B., Klotzli, U., Guntle, P., and Dragnits, E., 2001, The early Paleozoic magmatic events in the Northwest Himalaya, India: source, tectonic setting and age of emplacement. Geological Magazine, 138, 237–251.

Myrow, P.W., Snell, K.E., Hudges, N.C., Paulsen, T.S., Heim, N.A., and Parcha, S.K., 2006a, Cambrian depositional history of the Zanskar Valley region of the Indian Himalaya: tectonic implications. Journal of Sedimentary Research, 76, 364–381.

Myrow, P.W., Thompson, K.R., Hughes, N.C., Paulsen, T.S., Sell, B.K., and Parcha, S.K., 2006b, Cambrian stratigraphy and depositional history of the northern Indian Himalaya, Spiti Valley, north-central India. Geological Society of America Bulletin, 118, 491–510.

Naeem, M., 2013, Petrology of Mansehra Granitic Complex, Hazara area, NW Himalaya, Pakistan. Ph.D. Thesis, University of the Punjab, Lahore, 72 p.

Norrish, K. and Hutton, J.T., 1969, An accurate X-ray spectrographic method for the analysis of a wide range of geological samples. Geochimica et Cosmochimica Acta, 33, 431–453.

Okay, A.I., Satır, M., and Shang, C.K., 2008, Ordovician metagranitoid from the Anatolide–Tauride Block, northwest Turkey: geodynamic implications. Terra Nova, 20, 280–288.

Paudel, L.P. and Arita, K., 2000, Tectonic and polymetamorphic history of the Lesser Himalaya in Central Nepal. Journal of Asian Eartn Science, 18, 561–584.

Pupin, J.P., 1980, Zircon and granite petrology. Contributions to Mineralogy and Petrology, 73, 207–220.

Rahman, A., 1961, A gravity study of granites in the Mansehra area, West Pakistan. Geological Bulleton Punjab University, 1, 15–20.

Shah, S.M.I., 2009, Stratigraphy of Pakistan. Geological Survey of Pakistan (GSP), Ministry of Petroleum and Natural Resources, 22, 37 p.

Shams, F.A., 1961, A preliminary account of the geology of the Mansehra area, District Hazara, West Pakistan. Geological Bulletin of University of the Punjab, 1, 57–67.

Shams, F.A., 1967, A note on the ages of micas from some granites of the Mansehra-Amb State area, West Pakistan. Geological Bulletin of University of the Punjab, 6, 89–90.

Shams, F.A., 1971, The geology of the Mansehra-Amb State area, Northern West Pakistan. Geological Bulletin of University of the Punjab, 8, 1–31.

Shand, S.J., 1943, Eruptive Rocks. John Wiley & Sons, New York, 444 p.

Schärer, U. and Allègre, C.J., 1983, The Palung granite (Himalaya): high resolution U-Pb systematics in zircon and monazite. Earth and Planetary Science Letters, 63, 423–432.

Sorkhabi, B.R. and Arits, K., 1997, Tpwards a solution for the Himalaya puzzle: mechanism of inverted metamorphism constrained by the Siwalik sedimentary record. Current Scienec, 72, 862–873.

Stöcklin, J., 1980, Geology of Nepal and its regional frame. Journal of the Geological Society, 137, 1–34.

Streckeisen, A., 1974, Classification and nomenclature of plutonic rocks. Geologische Rundschau, 63, 773–786.

Tera, F. and Wasserburg, G. J., 1972, U-Th-Pb systematics in three Apollo 14 basalts and the problem of initial Pb in lunar rocks. Earth and Planetary Science Letters, 17, 281–304.

Trivedi, J.R., Gopalan, K., and Valadiya, K.S., 1984, Rb/Sr ages of granitic rocks within the Lesser Himalayan nappes, Kumaun, India. Journal of Geological Society of India, 25, 641–654.

Trivedi, J.R., 1990, Geochronological studies of Himalayan granitoids. Unpublished Ph.D. Thesis, Physical Research Laboratory, Ahmedabad, 170 p.

Ustaömer, P.A., Ustaömer, T., Alastair, G.A., Robertson, H.F., and Collins, A.S., 2012, Evidence of Precambrian sedimentation/magmatism and Cambrian metamorphism in the Bitlis Massif, SE Turkey utilizing whole-rock geochemistry and U-Pb LA-ICP-MS zircon dating. Gondwana Research, 21, 1001–1018.

Varva, G., Gebauer, D., Schmidt, R., and Compston, W., 1996, Multiple zircon growth and recryatallization during polyphase late Carboniferous to Triassic metamoprphism in granulites of the Ivrea Zone (south Alps): an ion microprobe (SHRIMP) study. Contributions to Mineralogy and Petrology, 122, 337–358.

Virjan, A.R., Dutta, D., Singh, M.P., Ghosh, N., Rathore, S.S., and Uniyal, A.K., 2003, Imprint of Himalayan Orogeny on Pan African Granitoid Intrusives: Evidence from Dhaoladhar Granite NW Himalaya, India. In: Singh, S. (ed.), Granitoids of the Himalayan Collisional Belt. Journal of the Virtual Explorer, Electronic Edition, Volume 11, Paper 04, ISSN 1441-8142.

Wadia, D.N., 1928, The geology of the Poonch State, Kashmir and adjacent parts of the Punjab. Memoirs of Geological Survey of India, 51, 233 p.

Wadia, D.N., 1957, Geology of India (3rd edition). Macmillan and Company, London, 531 p.

Wang, Y.Z., 2000, Tectonics and Mineralization of Southern Sanjiang Area. Geology Press, Beijing, 45–49.

Wang, B.D.,Wang, L.Q., Pan, G.T., Yin, F.G.,Wang, D.B., and Tang, Y., 2012a, U-Pb zircon dating of early Paleozoic gabbro from the Nantinghe ophiolite in the Changning–Menglian suture zone and its geological implication. Chinese Science Bulletin, 58, 344–354.

Wang, X.X., Zhang, J.J., Santosh, M., Yan, S.Y., and Guo, L., 2012b, Andean-type orogeny in the Himalayas of south Tibet: Implications for early Paleozoic tectonics along the Indian margin of Gondwana. Lithos, 154, 248–262.

Wang, Y., Xing, X., Cawood, P.A., Lai, S, Xia X., Fan, W., Liu, H., and Zhang, F., 2013, Petrogenesis of early Plaeozoic peraluminous granite in the Sibumasu Block of SW Yunnan and diachronous accretionary orogenesis along the northern margin of Gondwana. Lithos, 182–183, 67–85.

Williams, I.S., 1998, U-Th-Pb Geochronology by Ion Microprobe. In: McKibben, M.A., Shanks III, W.C., and Ridley, W.I. (eds.), Applications of Microanalytical Techniques to Understanding Mineralizing Processes. Reviews in Economic Geology, 7, p. 1–35.

Williamson, B.J., Downes, H., Thirlwall, M.F., and Beared, A., 1997, Geochemical constraints on restite composition and unmixing in the Velay anatectic granite, French Massif Central. Lithos, 40, 848–856.

Xu, Z.Q., Yang, J.S., Liang, F.H., Qi, X.X., Liu, F.L., Zeng, L.S., Liu, D.Y., Li, H.B., Wu, C.L., Shi, R.D., and Chen, S.Y., 2005, Pan-African and Early Paleozoic orogenic events in the Himalayan terrane: inference from SHRIMP U-Pb zircon ages. Acta Petrologica Sinica, 21, 1–12.

Zhang, Z.M., Wang, J.L., Shen, K., and Shi, C., 2008, Paleozoic circus-Gondwana orogens: petrology and geochronology of the Namche Barwa Complex in the eastern Himalayan syntaxis, Tibet. Acta Petrologica Sinica, 24, 1627–1637.

Zhou, Z.G., Liu, W.C., and Liang, D.Y., 2004, Discovery of the Ordo-

vician and its basal conglomerate in the Kangmar area, southern Tibet – with a discussion of the relation of the sedimentary cover and unifying basement in the Himalayas. Geological Bulletin of China, 23, 655–663.

Zhu, D.C., Zhao, Z.D., Niu, Y.L., Dilek, Y., Wang, Q., Ji, W.H., Dong, G.C., Sui, Q.L., Liu, Y.S., Yuan, H.L., and Mo, X.X., 2012, Cambrian bimodal volcanism in the Lhasa Terrane, southern Tibet: record of an early Paleozoic Andean-type magmatic arc in the Australian proto-Tethyan margin. Chemical Geology, 328, 290–308.

Manuscript received April 20, 2015
Manuscript accepted September 29, 2015